



CHALMERS

Chalmers Publication Library

Estimation of Forest Biomass From Two-Level Model Inversion of Single-Pass InSAR Data

This document has been downloaded from Chalmers Publication Library (CPL). It is the author's version of a work that was accepted for publication in:

Ieee Transactions on Geoscience and Remote Sensing (ISSN: 0196-2892)

Citation for the published paper:

Soja, M. ; Persson, H. ; Ulander, L. (2015) "Estimation of Forest Biomass From Two-Level Model Inversion of Single-Pass InSAR Data". Ieee Transactions on Geoscience and Remote Sensing, vol. 53(9), pp. 5083-5099.

<http://dx.doi.org/10.1109/tgrs.2015.2417205>

Downloaded from: <http://publications.lib.chalmers.se/publication/219664>

Notice: Changes introduced as a result of publishing processes such as copy-editing and formatting may not be reflected in this document. For a definitive version of this work, please refer to the published source. Please note that access to the published version might require a subscription.

Chalmers Publication Library (CPL) offers the possibility of retrieving research publications produced at Chalmers University of Technology. It covers all types of publications: articles, dissertations, licentiate theses, masters theses, conference papers, reports etc. Since 2006 it is the official tool for Chalmers official publication statistics. To ensure that Chalmers research results are disseminated as widely as possible, an Open Access Policy has been adopted. The CPL service is administrated and maintained by Chalmers Library.

(article starts on next page)

Estimation of Forest Biomass From Two-Level Model Inversion of Single-Pass InSAR Data

Maciej Jerzy Soja, Henrik J. Persson, and Lars M. H. Ulander, *Senior Member, IEEE*

Abstract—A model for aboveground biomass estimation from single-pass interferometric synthetic aperture radar (InSAR) data is presented. Forest height and canopy density estimates Δh and η_0 , respectively, obtained from two-level model (TLM) inversion, are used as biomass predictors. Eighteen bistatic VV-polarized TanDEM-X (TDM) acquisitions are used, made over two Swedish test sites in the summers of 2011, 2012, and 2013 (nominal incidence angle: 41° ; height-of-ambiguity: 32–63 m). Remningstorp features a hemiboreal forest in southern Sweden, with flat topography and where 32 circular plots have been sampled between 2010 and 2011 (area: 0.5 ha; biomass: 42–242 t/ha; height: 14–32 m). Krycklan features a boreal forest in northern Sweden, 720-km north–northeast from Remningstorp, with significant topography and where 31 stands have been sampled in 2008 (area: 2.4–26.3 ha; biomass: 23–183 t/ha; height: 7–21 m). A high-resolution digital terrain model has been used as ground reference during InSAR processing. For the aforementioned plots and stands and if the same acquisition is used for model training and validation, the new model explains 65%–89% of the observed variance, with root-mean-square error (RMSE) of 12%–19% (median: 15%). By fixing two of the three model parameters, accurate biomass estimation can also be done when different acquisitions or different test sites are used for model training and validation, with RMSE of 12%–56% (median: 17%). Compared with a simple scaling model computing biomass from the phase center elevation above ground, the proposed model shows significantly better performance in Remningstorp, as it accounts for the large canopy density variations caused by active management. In Krycklan, the two models show similar performance.

Index Terms—Aboveground biomass (AGB), canopy density, forest height, interferometric model, interferometric synthetic aperture radar (InSAR), TanDEM-X (TDM), two-level model (TLM).

I. INTRODUCTION

FORESTS are important natural resources because of their economic value and their crucial role in the local and global ecosystems [1]. Efficient and sustainable management

procedures are required to maintain healthy and productive forests.

One of the key elements in forest management is to have reliable information for short- and long-term planning. The aboveground dry biomass, here shortly called biomass or the AGB, is particularly important for carbon cycle studies, whereas parameters such as forest height and canopy density can both aid biomass estimation and provide additional information on the forests. However, current methods of collecting forest information are expensive, and cost-effective methods need to be developed. Remote sensing in combination with field inventories has the potential to meet these requirements and provide frequent and high-resolution mapping of forest variables. Large-scale mapping is also needed for natural disaster management and for the detection of unlawful deforestation.

Aerial photography has traditionally been used for forest mapping [2], [3]. This technique has the advantage of being relatively easy to implement and interpret but it requires cloud-free acquisitions and good flying weather. Moreover, it is less efficient on a large scale and whenever frequent updates are needed. Spaceborne photography is more efficient in terms of coverage and acquisition rate, but it has lower resolution. More advanced optical techniques, such as photogrammetry [4], [5], can provide additional information on forests, but the even stricter requirements on the acquired data make their use more difficult on an operational scale.

In recent years, airborne lidar scanning (ALS) has become popular. The technique uses laser pulses transmitted downwards from an airborne platform, which are used to sample height at high vertical and horizontal resolutions [4], [6]–[10]. Due to the high resolutions and the penetration of laser pulses through canopy gaps, ALS can provide information on both horizontal and vertical forest structures, and many important forest parameters can be derived from the data. ALS is today considered the most accurate remote sensing technique in forestry [10]. However, the technique is relatively expensive and thus inefficient for frequent and large-scale mapping. Spaceborne lidar, on the other hand, has yet unresolved resolution, coverage, and technology limitations [11].

SAR is an active remote sensing technique in which radio or microwave frequency pulses are used to probe the environment. Spaceborne SAR sensors can provide weather- and daylight-independent imagery of the Earth, and submeter resolutions are feasible. Through the choice of the center frequency, SAR systems can be optimized to fit different needs [12]. In forestry, low frequency bands, such as the VHF-band (30–300 MHz) and the lower UHF-band (300–1000 MHz,

Manuscript received July 11, 2014; revised December 19, 2014; accepted February 26, 2015. This work was supported in part by the Swedish National Space Board and in part by the European Union's Seventh Framework Programme (Advanced SAR) under Grant 606971.

M. J. Soja is with the Department of Earth and Space Sciences, Chalmers University of Technology, SE-412 96 Gothenburg, Sweden (e-mail: maciej.soja@chalmers.se).

H. J. Persson is with the Department of Forest Resource Management, Swedish University of Agricultural Sciences, SE-901 83 Umeå, Sweden.

L. M. H. Ulander is with the Department of Earth and Space Sciences, Chalmers University of Technology, SE-412 96 Gothenburg, Sweden, and also with the Radar Systems Unit, Swedish Defence Research Agency (FOI), SE-581 11 Linköping, Sweden.

Color versions of one or more of the figures in this paper are available online at <http://ieeexplore.ieee.org>.

Digital Object Identifier 10.1109/TGRS.2015.2417205

according to the IEEE standard) are more suitable for imaging of tree trunks and ground surface, whereas the high frequency bands, such as the X-band (8–12 GHz), are more suitable for imaging of tree canopies. SAR is one of the most promising tools for forest remote sensing, and many past and ongoing studies are dedicated to the retrieval of forest parameters from SAR data [13].

The TanDEM-X (TDM) system consists of two almost identical X-band SAR satellites flying in a tight tandem formation, at a distance of a few hundred meters during the main operational phase. Using the principles of InSAR, small phase differences between the two acquired SAR images are used to measure the position of the scattering center [14], i.e., to create a digital elevation model (DEM). With the tight tandem formation and bistatic-mode acquisitions of TDM, the temporal changes between the two SAR acquisitions are minimal, and the acquired height measurements are very precise.

The acquired DEM can be corrected for ground topography if a high-resolution digital terrain model (DTM) is available, and a map of the scattering center elevation above ground can be obtained. In Sweden, there is a national, lidar-scanned DTM with a grid posting of $2\text{ m} \times 2\text{ m}$ and height accuracy better than 0.5 m [15]. Similar DTMs exist or are being created in many other countries. Since the changes of the ground surface are very slow in most forested regions, only one lidar scanning is required to obtain a high-resolution DTM, and after that, mapping of forest canopy can be done with an InSAR system.

The exact position of the scattering center above ground in forests is related to the structure of the forest, and it depends on forest properties such as forest height and canopy density. In several studies, this relation has been investigated. In [16]–[18], the potential of C-band and X-band single-pass InSAR data acquired within the SRTM mission [19] has been evaluated for forest height estimation. In [20], [21], random volume over ground model inversion has been applied to estimate forest height from single-pass X-band InSAR data. In [22], a linear relation between biomass and the measured elevation of the scattering center above ground has been observed, following a similar study of X-band SRTM data [23]. In [24], biomass estimates have been obtained from ground-corrected TDM interferograms using the inversion of the interferometric water cloud model (IWCM). The IWCM includes an allometric relation between forest height and biomass, as well as temporal decorrelation modeling. Both interferometric coherence and phase, as well as backscatter intensity data, have been used in the inversion process. In [25], a multiple regression approach using interferometric height, coherence, and their transformed versions has been used to estimate biomass, separately for two test sites in Sweden.

In [26] and [27], it has been shown that direct inversion of a two-level model (TLM) can provide estimates of forest height and canopy density in a hemiboreal forest in Sweden. The main scope of this paper is to develop and evaluate a new model for biomass estimation from the inverted TLM parameters. Such a model can be used for large-scale biomass mapping in countries where national lidar scanning campaigns have been conducted. The performance of the proposed model is evaluated using multiple TDM acquisitions made during the summers of 2011,

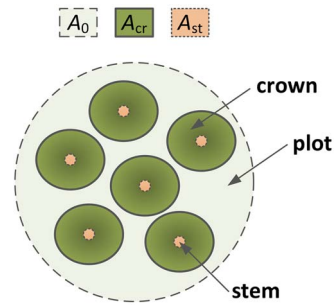


Fig. 1. Geometrical visualization of a forest plot.

2012, and 2013 over two boreal test sites in Sweden, separated by 720 km. The model is also compared with a simple scaling model (SM) presented in [22] and converting the phase center elevation above ground to biomass using a constant scaling factor.

II. MODELS

In this section, the basic models used in this paper will be described. First, it will be shown how biomass can be estimated from forest height and canopy density. Then, it will be shown how forest height and canopy density can be estimated from InSAR data. Thereafter, the results from the first two sections will be used together, and a new model for biomass estimation from InSAR data will be presented. Finally, the evaluation method used in this paper will be described, together with statistical tools for quantitative model performance assessment.

Note that, in this paper, the two terms “forest height” and “canopy density” are used as generic terms for different types of metrics quantifying forest height and fractional canopy density, respectively.

A. AGB from Forest Height and Canopy Density

Aboveground biomass (AGB) is defined as the total dry mass of all aboveground forest, most commonly measured in terms of biomass density, i.e., as mass per area unit. As a large part of the AGB is confined to the stem (around 3/4 for spruce and pine in Sweden, according to [28]), a geometrical argument [29], [30] suggests that the AGB can be estimated from the total volume of all stems using the following:

$$\widehat{\text{AGB}} = C \cdot h \cdot \frac{A_{\text{st}}}{A_0} \quad (1)$$

where C is a forest type-dependent constant (the product of a taper factor accounting for the noncylindrical trunk shape, the oven-dry wood density, and an expansion factor for the conversion of stem biomass to the total AGB), $h = \sum_{i=1}^N h_i A_i / \sum_{i=1}^N A_i$ is the Lorey’s height (basal area-weighted average of the individual tree heights h_i for N trees indexed with i and with individual basal areas A_i), $A_{\text{st}} = \sum_{i=1}^N A_i$ is the total basal area for all trees, and A_0 is the ground area of the plot, as visualized in Fig. 1.

In field inventories, the total basal area is estimated from stem diameter measurements. The measurement of forest height is more time-consuming, and many allometric equations for

biomass computation require only stem diameter measurements [30]–[32].

In remote sensing, there are several techniques for forest height estimation, including lidar scanning [7], [33], [34], polarimetric InSAR [35]–[37], photogrammetry [4], [5], and radargrammetry [38], [39], but the estimation of the basal area is difficult due to canopy closure, shadowing, and low resolution. On the other hand, the size of tree crowns can be estimated from, e.g., aerial photography [40]–[42] or ALS [9], [43], [44]. Since several studies show a reasonable correlation between canopy diameter and stem diameter for many tree species [45]–[47], the total crown area A_{cr} will be used in the following as a predictor of the total basal area, yielding

$$\widehat{AGB} = C' \cdot h \cdot \eta_{cr} \quad (2)$$

where $C' = C(A_{st}/A_{cr})$ is a forest type-dependent constant, and

$$\eta_{cr} = \frac{A_{cr}}{A_0} \quad (3)$$

is the canopy cover, which quantifies canopy density accounting for gaps between separate tree canopies but disregarding within-canopy gaps.

The main purpose of the argument above is to show that a multiplicative model is appropriate for biomass estimation from metrics related to forest height and canopy density. However, this argument is based on several simplifying assumptions regarding the shape of the trees, their intrinsic wood properties, their spatial distribution, tree parameter distribution within a plot, etc. In reality, the dependence of the AGB on the two forest parameters is expected to be more complicated. For instance, there will be a residual dependence of C' on height and basal area, which may affect the dependence of the AGB estimate in (2) on h and η_{cr} . Exponents α and β are therefore introduced to create an improved model, based on the experience from field inventories [30], [31], i.e.,

$$\widehat{AGB} = C'' \cdot h^\alpha \cdot \eta_{cr}^\beta \quad (4)$$

where C'' is a new forest type-dependent constant.

In the following, the Lorey's height h and the canopy cover η_{cr} in (4) will be replaced by related metrics obtained from InSAR.

B. Forest Height and Canopy Density from InSAR

In InSAR [14], the complex correlation coefficient is the main observable, and it is defined as

$$\tilde{\gamma} = \frac{E[s_1 s_2^*]}{\sqrt{E[|s_1|^2] E[|s_2|^2]}} \quad (5)$$

where s_1 and s_2 are the two interferometric images, $*$ is the complex conjugate operator, and $E[\bullet]$ is the expectation value operator.

Coherence is the magnitude of the complex correlation coefficient, and it is a measure of similarity between two images. The phase of the correlation coefficient carries information

about the vertical distribution of the scatterers. In applications, the complex correlation coefficient is estimated from a finite number of samples, and the interferometric phase is affected by noise. The total noise level will increase with a decreasing number of independent samples and/or decreasing coherence [48].

The loss of coherence (decorrelation) can be caused by up to four different effects: temporal changes in the scene, geometric differences between the two images, thermal noise, and system imperfections [49], [50]. In this paper, only the second effect will be studied, whereas the other three effects will be neglected.

Volume decorrelation is a geometric effect caused by the distribution of scatterers in the vertical direction z . It can be modeled from the vertical backscattering profile $\sigma_z(z)$ using [51], [52]

$$\tilde{\gamma}_{vol} = \frac{\int_{-\infty}^{\infty} \sigma_z(z) e^{ik_z z} dz}{\int_{-\infty}^{\infty} \sigma_z(z) dz} \quad (6)$$

with k_z being the vertical wavenumber, which for a bistatic acquisition geometry is

$$k_z = \frac{2\pi}{HOA} = \frac{2\pi B_\perp}{\lambda R \sin \theta} \quad (7)$$

where HOA is the height of ambiguity, B_\perp is the perpendicular baseline, λ is the wavelength, R is the average range, and θ is the average angle of incidence. HOA is the height corresponding to a 2π -phase shift in the interferogram, and it is the maximal height difference that can be unambiguously resolved by the interferometric system.

In the TLM [26], [27], [53], forest is modeled as two scattering levels, i.e., ground and vegetation, with the respective backscattering coefficients σ_{gr}^0 and σ_{veg}^0 . If the level distance is denoted by Δh and the elevation of the ground level is represented by z_0 , the vertical backscattering profile $\sigma_z(z)$ becomes

$$\sigma_z(z) = (1 - \eta)\sigma_{gr}^0 \delta(z - z_0) + \eta\sigma_{veg}^0 \delta(z - (z_0 + \Delta h)) \quad (8)$$

where $\delta(\bullet)$ is the Dirac delta function, and η represents the fraction of the total area covered by the vegetation level, thus being a measure of canopy density accounting both for the openings between separate tree canopies and for within-canopy gaps. In the following, η will be called an area-fill factor, which is the name used in works related to the IWCM, where it was originally introduced [24], [52], [54].

Inserting (8) in (6) yields

$$\tilde{\gamma}_{vol} = e^{ik_z z_0} \cdot \frac{\mu + e^{ik_z \Delta h}}{\mu + 1} \quad (9)$$

where

$$\mu = \rho \cdot \frac{1 - \eta}{\eta} \quad (10)$$

is the area-weighted backscatter ratio, and where the ground-to-vegetation backscatter ratio ρ is defined as

$$\rho = \frac{\sigma_{gr}^0}{\sigma_{veg}^0}. \quad (11)$$

The first exponential term in the expression for the TLM in (9) introduces a phase term related to the ground topography z_0 . This phase term can also be observed in the measured complex correlation coefficient $\tilde{\gamma}$. If ground topography is known, e.g., from an external DTM, then this exponential term can be used to compensate the complex correlation coefficient for ground topography, so that the ground-corrected complex correlation coefficient can be obtained, i.e.,

$$\tilde{\gamma}_{gc} = \frac{E [s_1 s_2^* e^{-ik_z z_0}]}{\sqrt{E [|s_1|^2] E [|s_2|^2]}}. \quad (12)$$

In this paper, the term ‘‘ground-corrected’’ indicates that the phase variations caused by ground topography have been removed from the complex correlation coefficient using a high-resolution DTM. The magnitude of the ground-corrected complex correlation coefficient is the ground-corrected coherence, in the following referred to as $\gamma_{gc} = |\tilde{\gamma}_{gc}|$.

From the phase of the ground-corrected complex correlation coefficient $\tilde{\gamma}_{gc}$, the interferometric height (scattering phase center elevation above ground) can be obtained using the following:

$$h_{gc} = \frac{\arg(\tilde{\gamma}_{gc}) + 2\pi n}{k_z} = \text{HOA} \left(\frac{\arg(\tilde{\gamma}_{gc})}{2\pi} + n \right) \quad (13)$$

where $\arg(\bullet)$ is the argument operator, and the integer n describes the ambiguity of the phase computation.

Note that, in many studies, including [16]–[18], [22], [23], the phase center elevation above ground is estimated by subtracting a high-resolution DTM from a DEM obtained from InSAR, i.e., by first creating a height model from the interferometric phase (which includes the variations due to ground topography), and then removing the topographic variations. In (12) and (13), the interferogram is first compensated for the topographic variations, and then the interferometric phase is converted to height. The presented approach has several advantages: decorrelation due to topographic phase variations in the averaged pixels is minimized, processing does not rely on advanced phase unwrapping techniques, and the produced estimate of the phase center height is potentially more accurate as the risk of wrapping errors is reduced, coherence is maximized, and the averaging in (12) can be done on plot or stand level, meaning that the number of independent complex looks can be maximized (see also Section III-G).

In the absence of decorrelation effects other than volume decorrelation, the measured ground-corrected complex correlation coefficient $\tilde{\gamma}_{gc}$ can be modeled by the TLM expression in (9) with $z_0 = 0$, i.e.,

$$\tilde{\gamma}_{gc} = \frac{\mu + e^{ik_z \Delta h}}{\mu + 1}. \quad (14)$$

Since this equation has two unknowns (Δh and μ) and two observables (the real and imaginary parts of $\tilde{\gamma}_{gc}$), it can be solved without the need for multiple acquisitions. The TLM describes a circle in the complex plane with its center on the

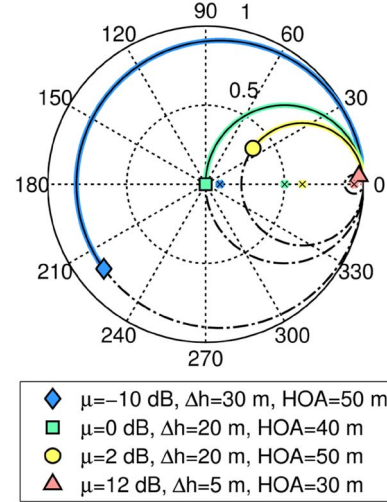


Fig. 2. Inversion of the TLM consists of finding a circle passing through unity and $\tilde{\gamma}_{gc}$, and with its center on the positive x -axis. In this figure, the TLM inversion is visualized using four hypothetical cases with different μ , Δh , and HOA values. Circle centers are shown with crosses.

positive x -axis and passing through unity and $\tilde{\gamma}_{gc}$ (see Fig. 2). Explicit solutions for Δh and μ are readily available, i.e.,

$$\Delta h = \frac{1}{k_z} \left(\tan^{-1} \left[\frac{2\text{Im}[\tilde{\gamma}_{gc}] (1 - \text{Re}[\tilde{\gamma}_{gc}])}{2\text{Re}[\tilde{\gamma}_{gc}] (1 - \text{Re}[\tilde{\gamma}_{gc}]) + \gamma_{gc}^2 - 1} \right] + \pi n \right) \quad (15)$$

$$\mu = \frac{1 - \gamma_{gc}^2}{1 - 2\text{Re}[\tilde{\gamma}_{gc}] + \gamma_{gc}^2} \quad (16)$$

where $\text{Re}[\bullet]$ and $\text{Im}[\bullet]$ are the real and imaginary part operators, respectively, and n is an integer describing the ambiguity of the inversion. The lowest positive Δh is chosen in cases when HOA is larger than forest height.

In [26] and [27], it has been shown that Δh estimated from VV-polarized TDM data is correlated with H95 and H50, which are two lidar metrics for forest height computed as the 95th and 50th percentile, respectively, of lidar returns above a threshold of 1 m or 10% of the maximal lidar return. It has also been shown in [26] and [27] that the uncorrected area-fill factor defined and computed as

$$\eta_0 = \frac{1}{1 + \mu} = \frac{\frac{1}{2} (1 + \gamma_{gc}^2) - \text{Re}[\tilde{\gamma}_{gc}]}{1 - \text{Re}[\tilde{\gamma}_{gc}]} \quad (17)$$

is correlated with the vegetation ratio (VR), which is a lidar metric for canopy density computed as the fraction of all lidar returns originating from above 1 m or 10% of the maximal lidar height (see [55]). The uncorrected area-fill factor can be obtained by solving (10) for η under the assumption that $\rho = 1$. The validity of this assumption has been discussed in [26], and it has been concluded that, at high frequencies, such as for the X-band data used in [26] and [27], the ground-level and vegetation-level scattering coefficients are similar as the wavelength is short compared with the size of the scatterers and the orientation of the scatterers can be considered random.

As aforementioned, the derivation of (16), (15), and (17) is based on the assumption that the total decorrelation is solely caused by the volume effect. In the TDM system used in this

paper, the near-simultaneous bistatic acquisition scenario minimizes the temporal decorrelation [56]. Common-band filtering of both interferometric images deals with most of the spatial decorrelation effect caused by different range and Doppler frequency bands [57]. Therefore, the two most significant decorrelation effects other than volume decorrelation are caused by the finite SNR and the system imperfections. In [56], the total coherence for soil and rock for VV-polarized TDM acquisitions in mid-swath and at a 41° incidence angle has been modeled to approximately 0.88 for an occurrence level of 50% and 0.82 for an occurrence level of 90%. In this paper, however, all decorrelation effects other than volume decorrelation will be neglected for practical reasons, and the validity of this assumption will be discussed in Section V.

Due to the high resolution of TDM data and relatively large regions of interests, a large number of independent samples can be used during the estimation of the complex correlation coefficient, and the errors in coherence and phase estimation are negligible. An estimate of the number of looks used during the computation of the complex correlation coefficient will be given in Section III-G.

C. Biomass Models

As the TLM parameters Δh and η_0 have been found correlated with lidar-based metrics of forest height and canopy density, it is reasonable to use them in (4), which yields the TLM biomass model (TBM), i.e.,

$$\widehat{\text{AGB}} = K \cdot \Delta h^\alpha \cdot \eta_0^\beta \quad (18)$$

where K , α , and β are unknown model parameters.

The TBM will be compared with a linear zero-intercept model, which scales the interferometric forest height h_{gc} to biomass, i.e.,

$$\widehat{\text{AGB}} = D \cdot h_{gc} \quad (19)$$

where D is a scaling factor, which needs to be estimated from training data. This model has been proposed in [22]. In the following, it will be referred to as the scaling model, or simply the SM.

D. Evaluation Strategy

The models will be evaluated using multiple TDM acquisitions made over two geographically separated test sites in Sweden, during three consecutive summers and at different HOAs. The models will be tested both for their explanatory values (that is how well they can be fitted to the data) and their predictive values (that is how well they can predict biomass from other data). The models will thus be tested for their robustness to the change of test site, acquisition year, and acquisition HOA. They will also be used to produce biomass maps, to see how well the spatial variations can be reproduced.

The significance of each model parameter will be studied using the Student's t -test. This test evaluates the hypothesis

that the expectation value of the normally distributed parameter estimate $\hat{\beta}$ is β_0 . The t -statistic is computed as

$$t = \frac{\hat{\beta} - \beta_0}{\hat{\sigma}_\beta} \quad (20)$$

where $\hat{\sigma}_\beta$ is the estimated standard deviation of $\hat{\beta}$. The Student's t -test will here be used to test the hypothesis that $\beta_0 = 0$. For a known number of degrees of freedom, the probability p of obtaining a certain t -statistic can be computed from the t -distribution. A low p -value means that β is a significant parameter.

The goodness-of-fit of each model will be evaluated using the coefficient of determination R^2 , which describes the fraction of the total variability observed in the data that can be explained by the model, i.e.,

$$R^2 = 1 - \frac{\sum_{i=1}^n (Y_i - \hat{Y}_i)^2}{\sum_{i=1}^n (Y_i - \bar{Y})^2} \quad (21)$$

where Y_i are the individual values of n observations indexed with i , \hat{Y}_i are the corresponding modeled values, and $\bar{Y} = (1/n) \sum_{i=1}^n Y_i$ is the average observed value.

The model error will be evaluated using the root-mean-square error (RMSE), which is computed as

$$\text{RMSE} = \sqrt{\frac{1}{n} \sum_{i=1}^n (Y_i - \hat{Y}_i)^2} \quad (22)$$

The fitting of the models has been done using nonlinear least squares, as implemented in the `nls`-function provided within the R-package [58]. Although the use of linear least squares is possible for the TBM model after a logarithmic transform, nonlinear regression has in many cases provided lower RMSE and larger R^2 , and it is therefore used throughout this paper.

III. DATA

A. Test Sites

Remningstorp is a hemiboreal test site situated in southern Sweden (58° 28' N, 13° 38' E; see Fig. 3). It is fairly flat with ground slopes at stand level lower than 5° (computed from a 50 m × 50 m DTM). The test site covers approximately 1200 ha of productive forest land, and the forest consists primarily of Norway spruce (*Picea abies* (L.) Karst.), Scots pine (*Pinus sylvestris* L.), and birch (*Betula* spp.) [55].

Krycklan is a boreal test site located in northern Sweden (64° 14' N, 19° 46' E; see Fig. 3). Krycklan is situated 720-km north-northeast of Remningstorp. Unlike Remningstorp, Krycklan has a strongly undulating topography with ground slopes on stand level up to 19° (again, computed from a 50 m × 50 m DTM). The forest is dominated by Norway spruce and Scots pine [59].

B. In Situ Data

A set of 32 circular, 0.5-ha plots (radius: 40 m) is available for Remningstorp. Field inventories were conducted during the autumn of 2010 and spring of 2011. For each plot, all



Fig. 3. Location of the two test sites Remningstorp and Krycklan used in this paper. The neighboring cities of Gothenburg and Umeå are also shown.

trees with a diameter at breast height (dbh) higher than 5 cm were calipered, and tree species were determined. Height was measured for a subset of roughly 10% of the trees. Out of the 32 plots and at the time of the inventories, 21 were spruce dominated (more than two-third of biomass), 5 were pine dominated, and 2 were birch dominated. Three plots consisted of a mixed spruce and pine forest and one plot consisted of a mixed forest with all three tree species. The stem number density of the 32 plots in Remningstorp was at the time of the inventories between 110 and 548 trees per hectare.

In Krycklan, 31 stands of irregular shape and sizes between 2.4 and 26.3 ha were inventoried in the summer of 2008. Systematic grids of circular field plots (radius 10 m) were laid out in each stand. The spacing of each grid was selected to give between 8 and 13 field plots per stand. For each field plot, all trees with a dbh higher than 4 cm were calipered, and tree species were determined. Tree height and age were also measured for 1–2 randomly chosen sample trees in each field plot. Of the 31 stands and at the time of the inventories, 5 were spruce dominated, 13 were pine dominated, 3 were mixed coniferous, and the remaining 10 were mixed forest stands. Compared with Remningstorp, the stands in Krycklan consist of smaller trees but in larger numbers, with stem number densities at the time of the inventories between 596 and 2543 trees per hectare.

C. Biomass Estimates

For both test sites, estimates of aboveground dry biomass have been made from the *in situ* data using the Heureka system [60], which implements the allometric functions described in

[28]. The allometric functions have been derived using multiple regression analysis of data from 1286 trees (Norway spruce, Scots pine, and birch) from 131 stands located across Sweden and described in [61] and [62].

Stem volume growth has been modeled in Heureka using the radial growth functions described in [28]. Although the SAR acquisitions have been made in the summer, which is in the middle of a growth season, biomass estimates for the end of the preceding growth season are used throughout this paper. The performance of the volume growth model used in Heureka has been evaluated in [63] using 1711 permanent plots from the National Forest Inventory (NFI) database. The prediction error (RMSE) for the stem volume has been found to be around 15%, and a small underestimation (bias) of 2% has been observed for spruce. Due to the close relation between forest volume and aboveground dry biomass, similar errors are also expected for the AGB.

A realistic estimate of the uncertainty in the reference biomass data used in this study is 15%, primarily based on the results presented in [63] and the errors presented in [28]. Although the sampling procedures in Remningstorp and Krycklan include dbh measurements for a large set of trees (all trees with dbh larger than 5 cm in Remningstorp), height has only been measured for a subset of trees and thereafter extrapolated to the other trees using regression from the dbh. Since both dbh and height are used for biomass estimation, the input variables to the allometric equations are correlated, which increases the uncertainty of the aggregated estimates. A possible site-dependent bias will also occur when the models presented in [28] are used locally, on data which may deviate from the data used for the derivation of these models. Additional uncertainties, such as *in situ* measurement errors and errors introduced during the determination of plot areas also contribute to the total error. Note that, in [64] and [65], the reported biomass estimation uncertainties are generally lower for similarly measured plots and stands. However, these estimates do not account for growth model errors and the site-dependent bias, which has been included in the 15%-error level used in this paper.

D. Forest Change Detection

After field measurements, several plots/stands have been altered through clearing, thinning, or clear-cutting. In Remningstorp, the altered plots have been identified using lists of management procedures provided by the managing company, SPOT-5 image analysis, and field visits. Three plots have been altered between the SAR acquisitions from 2011 and 2012, and additional eight between the SAR acquisitions from 2012 and 2013. In Krycklan, only SPOT-5 image analysis has been used. Two stands have been altered already before the first SAR acquisition in 2011, but no changes have been detected after that. Altered plots/stands have been disregarded in this paper.

E. Lidar Data

Airborne lidar scanning data acquired and processed within the BioSAR 2008 and 2010 campaigns [55], [59] have been used in this paper. In Krycklan, the lidar scanning data were

TABLE I
SUMMARY FOR THE EXPERIMENTAL DATA USED IN THIS PAPER. MEAN VALUES FOR ALL PLOTS ARE GIVEN. BACKGROUND SHADING HAS BEEN APPLIED ACCORDING TO HOA. N IS THE NUMBER OF AVAILABLE PLOTS/STANDS FOR EACH ACQUISITION

Nr	Site	Date	InSAR data			<i>In situ</i> & lidar data						
			B_{\perp} [m]	HOA [m]	Coherence	N	Biomass [t/ha]			H95 [m]		
							min	mean	max	min	mean	max
1	Remningstorp	20110604	282	49	0.65	32	42	148	242	14	23	32
2		20110809	266	52	0.67	28	42	150	242	14	23	32
3		20110820	258	54	0.66							
4		20120601	432	32	0.54	29	42	145	242	14	22	30
5		20120828	370	37	0.54							
6		20130702	270	51	0.66	21	42	143	242	14	22	30
7		20130724	226	61	0.73							
8		20130804	220	63	0.73							
9	Krycklan	20110617	258	52	0.71	29	23	94	183	7	16	21
10		20110720	250	54	0.75							
11		20110811	242	55	0.76							
12		20110822	240	56	0.78							
13		20120717	374	36	0.59							
14		20120808	360	37	0.61							
15		20120819	350	39	0.62							
16		20130601	270	50	0.73							
17		20130623	260	52	0.71							
18	20130726	216	62	0.79								

Color coding by HOA: 30 m 40 m 50 m 60 m

acquired between the 5th and 6th of August 2008, whereas in Remningstorp, the lidar acquisitions were made on the 29th of August 2010. Thereafter, DTMs created from lidar returns classified as ground with a designated classification algorithm [66], [67] were subtracted from digital surface models of the canopy created from lidar returns classified as vegetation, yielding digital canopy models (DCMs). From these DCMs, $10\text{ m} \times 10\text{ m}$ maps of several different lidar metrics were created. For the two test sites studied in this paper, H95 and VR are the two main biomass predictors used in lidar-based biomass mapping [55], [59], and they are therefore in focus in this paper. The 95th-percentile forest height, called H95, has been computed as the 95th percentile of all lidar returns above a threshold of 1 m or 10% of the maximal return within a $10\text{ m} \times 10\text{ m}$ cell. The lidar vegetation ratio, called VR, has been computed as the ratio between the number of returns from above that threshold to all returns. The VR is thus a measure of canopy density, accounting for both within-canopy gaps and the gaps between separate trees.

Biomass maps with a $10\text{ m} \times 10\text{ m}$ grid have been created using multiple regression analysis of different lidar metrics and species stratification maps (see [55] and [59]). In Remningstorp, 212 circular field plots with a radius of 10 m and distributed in a systematic grid over the entire test site have been used for model training. In Krycklan, the previously mentioned field plots located within the 31 stands, together with additional 110 circular field plots surveyed with the same methodology and positioned within the central part of the test site, have been used for model training. The uncertainty in the biomass maps is estimated to 20%, based on the uncertainties reported in [55], [59] and also accounting for a bias caused by the fact that growth has not been modeled in lidar data. Since the lidar data are only used in qualitative comparisons, this does not affect the quantitative results presented in this study.

F. DTM

As ground-level reference, the national lidar-scanned DTM acquired by the Swedish Land Survey is used [15]. The DTM has a $2\text{ m} \times 2\text{ m}$ grid, with a mean height error lower than 0.5 m. Lidar scanning has been performed from an airplane flying at an altitude between 1700 and 2300 m, with a point density on the ground between 0.5 and 1 point per square meter. In the southern part of the country, lidar scanning has primarily been performed during nonvegetative periods to minimize the contribution of leaves, grass, crops, etc.

G. InSAR Data

TanDEM-X (TDM) is a twin-satellite X-band (9.65 GHz) SAR interferometer in which acquisitions are made almost simultaneously [56]. Bistatic-interferometric, VV-polarized, stripmap mode TDM acquisitions made in the ascending mode with HOAs in the interval 32–63 m are used in this paper. This particular choice of HOA is motivated by the better sensitivity to forest height [68] and the relatively low risk of multiple phase wrapping in boreal forests. A summary of the data can be found in Table I, where background color coding by HOA has been applied. Note that the data from 2012 feature lower HOAs than the data from 2011 and 2013. The nominal angle of incidence varies between 41.2° and 41.7° for Remningstorp and between 40.4° and 41° for Krycklan. For images 1 and 9 in Table I (the first acquisitions for each test site), the scene center resolutions provided by the DLR in the meta files are: 1.8 m in ground range and 6.6 m in azimuth. For the rest of the images, the ground range resolution is 2.7 m and the azimuth resolution is 3.3 m.

The InSAR data have been interferometrically processed using an in-house developed algorithm based on [57]. The raw interferograms have been ground corrected in radar geometry

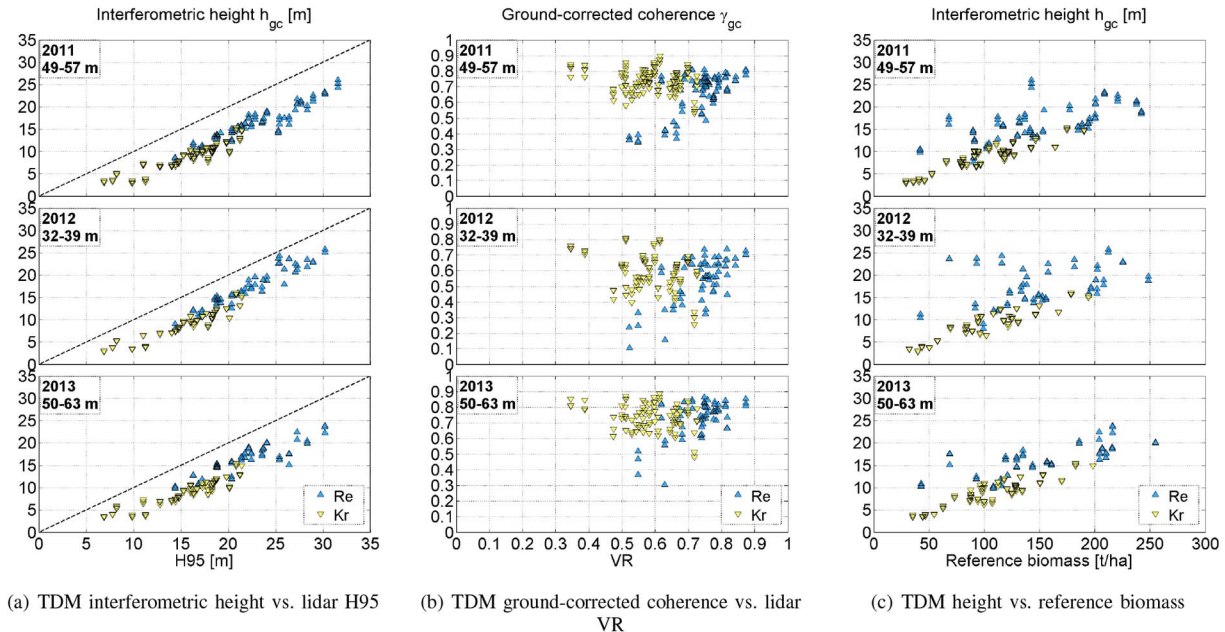


Fig. 4. TDM interferometric height and ground-corrected coherence are plotted against reference data. Acquisition year and HOA intervals are shown for each subplot. The points shown represent 0.5-ha plots in Remningstorp and 2.4–26.3-ha stands in Krycklan. Note that several points may overlap. In Remningstorp, there are 88 points in 2011, 58 points in 2012, and 63 points in 2013, whereas in Krycklan, there are 116 points in 2011 and 87 points in both 2012 and 2013.

using a linearly interpolated DTM and taking into consideration the quasi-bistatic acquisition geometry and satellite displacement between transmission and reception of the signals. A 5-m buffer zone has been added prior to plot/stand-level averaging of the ground-corrected interferograms. The lowest number of looks has been estimated to 320, computed as the ratio between the area of the smallest plot/stand in the data set (excluding the buffer zone), and the ground range and azimuth resolutions for the image with the lowest resolution. Absolute phase calibration has been done using ground reference points derived from a nonforest mask. No unwrapping has been found necessary due to the limited height variations in the flattened interferogram. Geocoding error and height measurement errors have been estimated using two 5-m trihedral corner reflectors situated within the Remningstorp site. The geocoding offset has been found lower than 2 m, and the standard deviation of the measured elevation of the scattering center has been found lower than 10 cm. For the creation of the ground-corrected coherence and height images, a 5×5 averaging window has been used.

IV. RESULTS

This section begins with a presentation of the interferometric observables obtained from TDM. Thereafter, TLM inversion results are presented, followed by regression results. Finally, biomass estimation is evaluated both for the TBM and for the SM, and sample biomass maps are shown for both models and both test sites, and compared with lidar-derived reference maps.

A. Interferometric Height and Coherence

In Fig. 4(a), TDM interferometric height h_{gc} is plotted against lidar height H95, separately for each year. A good

correlation can be observed, but the interferometric height is approximately 5–10 m lower for almost all stands.

For some Remningstorp plots with H95 just above 25 m, the interferometric height is approximately 5 m higher for the 2012 acquisitions (with HOAs equal to 32 m and 37 m) than for the 2011 and 2013 acquisitions (with HOAs around and above 50 m). This effect has previously been discussed in [26], where it has been concluded that it is caused by an interference effect occurring when ground- and vegetation-level scattering is of similar strength and when the distance between the respective scattering centers is around HOA/2. The affected plots consist of former seed trees with new understorey vegetation. The trees are sparse and allow for a significant penetration through the gaps, and the understorey vegetation layer boosts the ground-level scattering.

In Fig. 4(b), ground-corrected TDM coherence γ_{gc} is plotted against lidar vegetation ratio, separately for each year. It can be observed that coherence is consistently lower for the acquisitions from 2012 than for the other two acquisitions, due to the larger baseline, and for some plots, the coherence falls below 0.3. It is noted that these plots are the same, i.e., sparse plots with former seed trees and rich understorey vegetation, and that this low coherence occurs due to the aforementioned interference effect.

In Fig. 4(c), TDM interferometric height is plotted against reference biomass. For Krycklan, there is a good correlation between the interferometric height and biomass. For Remningstorp, however, there is a large height variance, particularly in the case of the data from 2012, with low HOA. It is noted that the plots with relatively low biomass but high interferometric height are the same sparse plots that have been discussed earlier. Note that one of these plots has been

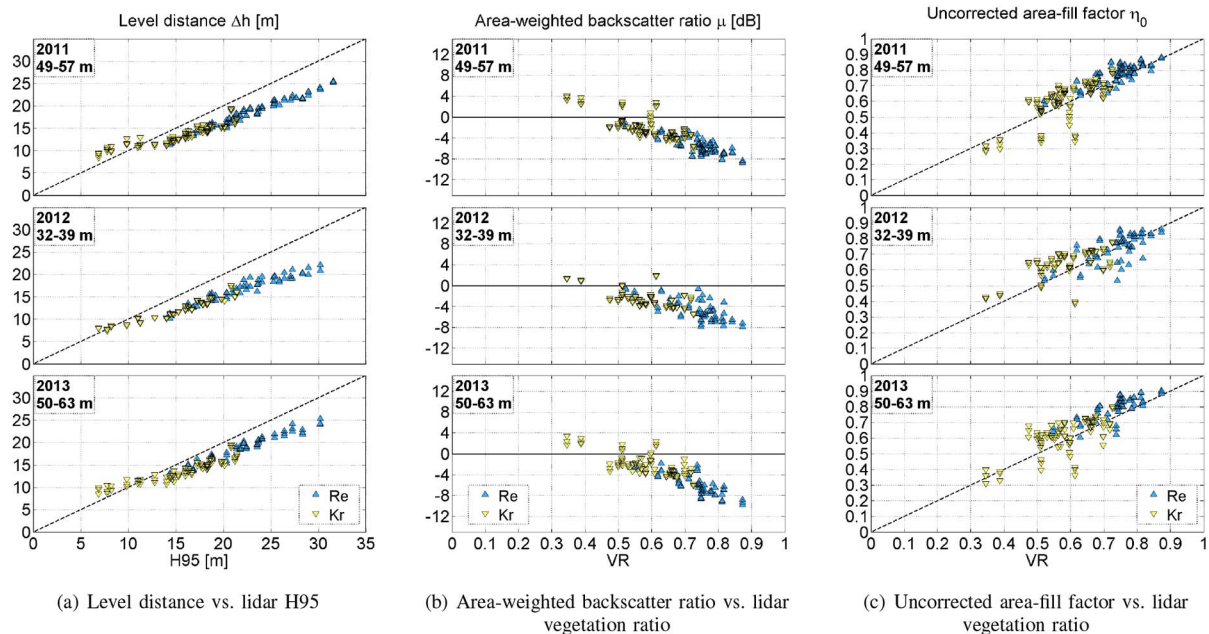


Fig. 5. Inverted TLM parameters are plotted against the reference data. Acquisition year and HOA intervals are shown for each subplot. The points shown represent 0.5-ha plots in Remningstorp and 2.4–26.3-ha stands in Krycklan. Note that several points may overlap. In Remningstorp, there are 88 points in 2011, 58 points in 2012, and 63 points in 2013, whereas in Krycklan, there are 116 points in 2011 and 87 points in both 2012 and 2013.

altered in 2012 and additional two in 2013, as described in [26], and they are not included in the scatter plots from 2012 and 2013.

B. TLM Inversion

In Fig. 5(a), the level distance Δh inverted using (15) is plotted against lidar height H95. It can be observed that the correlation between Δh and H95 is better than between the interferometric height and H95, but the bias is different, as observed in [26] and [27]. Note that the slope of the inverted level distance Δh changes at low H95. The reason for this will be discussed in Section V. Note that, in [26], Δh is also compared with H50 (the median of all lidar returns above 1 m or 10% of the maximal height), and it is observed that H50 and Δh are similar height metrics. H50 is not studied here as this paper is concentrated on biomass estimation, and H95 is the primary height metric used for that purpose in BioSAR 2008 and 2010 [55], [59].

In Fig. 5(b), the area-weighted backscatter ratio μ inverted using (16) is plotted in decibels against lidar vegetation ratio. Although these two parameters measure different properties, a good correlation can be observed.

In Fig. 5(c), the uncorrected area-fill factor η_0 inverted using (17) is plotted against lidar vegetation ratio. The correlation is good for most stands.

C. Model Parameter Estimation

In Table II, estimates of K , α , and β are shown for the TBM. The TBM is able to explain between 65% and 89% of the variance observed in the data. It can be observed that α is similar for both test sites and for most acquisitions, with

most values close to one. The other exponent β is similar for all acquisitions made over the same test site, but it changes between the test sites. For acquisitions made in Krycklan, it is close to one, whereas for those made in Remningstorp, it is closer to three. The third parameter K shows a large variance with values between 0.4 and 27.1.

Based on these observations, it is reasonable to let the exponents become constants. Exponent α is fixed to the same value for both test sites, whereas exponent β is made a site-dependent constant. In Table III(a), regression results for the TBM with α fixed to 1.25, and β fixed to 2.64 for Remningstorp and 1.16 for Krycklan are shown. The chosen values are all average values for the estimates presented in Table II. The estimated values of the slope constant K' are more stable than the estimates of K , between 6.6 and 10.2, without any significant difference between the two test sites. Note that the lowest R^2 is obtained for the image from Remningstorp with the lowest HOA. Since the choice of the fixed parameters is based on the mean of all values, it is biased toward acquisitions with large HOA, which are more frequent.

In Table III(b), regression results for the SM are shown. It can be observed that the slope is very stable for both Remningstorp and Krycklan, but it changes between the two sites. For Remningstorp, it is between 8.3 and 9.6, whereas for Krycklan, it is between 11.3 and 12.2. The two lowest values are obtained for the images over Remningstorp acquired at the lowest HOA values. For these, the coefficient of determination is -0.07 and 0.13 , and the SM is not able to explain the variance for these acquisitions.

Note that the fixed parameters chosen above as averages of the estimated parameters shown in Table II can also be estimated from regression of all relevant data, but this approach has not been chosen here. The main purpose of this part is to

TABLE II
RESULTS FOR THE TBM. FOR EACH PARAMETER, THE ESTIMATED STANDARD DEVIATIONS σ , t -STATISTICS, AND p -VALUES ARE SHOWN. FOR THE WHOLE MODEL, THE COEFFICIENTS OF DETERMINATION R^2 ARE SHOWN

$$\text{TBM: } \widehat{\text{AGB}} = K \cdot \Delta h^\alpha \cdot \eta_0^\beta$$

Nr	Site	K	σ	t	p	α	σ	t	p	β	σ	t	p	R^2
1	Remningstorp	9.4	4.87	1.9	6.4e-02	1.2	0.18	6.7	2.6e-07	2.7	0.37	7.3	4.5e-08	0.78
2		11.6	6.49	1.8	8.6e-02	1.1	0.19	6.0	3.3e-06	3.0	0.39	7.6	5.5e-08	0.81
3		27.1	15.39	1.8	9.1e-02	0.9	0.19	4.6	9.6e-05	3.0	0.38	7.9	3.0e-08	0.82
4		0.4	0.37	1.0	3.5e-01	2.4	0.39	6.0	2.2e-06	1.8	0.34	5.3	1.4e-05	0.65
5		1.7	1.13	1.5	1.5e-01	1.8	0.24	7.3	9.2e-08	2.0	0.30	6.5	7.4e-07	0.76
6		7.4	5.63	1.3	2.0e-01	1.2	0.25	4.8	1.3e-04	2.6	0.44	5.8	1.8e-05	0.81
7		6.5	3.71	1.7	9.8e-02	1.3	0.19	6.8	2.4e-06	2.9	0.36	8.0	2.4e-07	0.89
8		20.1	15.34	1.3	2.1e-01	0.9	0.25	3.8	1.2e-03	3.2	0.55	5.8	1.7e-05	0.81
9	Krycklan	15.0	11.34	1.3	2.0e-01	1.0	0.25	3.9	5.7e-04	1.4	0.26	5.5	9.4e-06	0.85
10		9.6	6.76	1.4	1.7e-01	1.1	0.23	4.8	5.8e-05	1.3	0.28	4.5	1.3e-04	0.84
11		13.7	9.25	1.5	1.5e-01	1.0	0.22	4.6	1.1e-04	1.4	0.27	5.2	2.2e-05	0.86
12		8.5	5.09	1.7	1.1e-01	1.2	0.21	5.7	5.8e-06	1.2	0.24	5.0	3.3e-05	0.87
13		3.9	2.37	1.6	1.2e-01	1.5	0.21	6.9	2.4e-07	0.9	0.34	2.6	1.6e-02	0.82
14		4.6	2.96	1.5	1.3e-01	1.4	0.22	6.4	8.3e-07	1.9	0.35	2.6	1.5e-02	0.82
15		6.7	4.53	1.5	1.5e-01	1.3	0.22	5.7	4.9e-06	1.2	0.38	3.0	5.4e-03	0.82
16		8.9	6.47	1.4	1.8e-01	1.1	0.24	4.8	5.4e-05	1.1	0.35	3.1	4.8e-03	0.81
17		20.5	16.41	1.2	2.2e-01	0.9	0.26	3.4	2.1e-03	1.4	0.28	4.9	4.9e-05	0.84
18	8.8	6.21	1.4	1.7e-01	1.1	0.24	4.8	5.5e-05	1.0	0.26	4.0	5.0e-04	0.83	

Color coding for acquisition number by HOA: 30 m 40 m 50 m 60 m

TABLE III
RESULTS FOR THE TBM WITH FIXED EXPONENTS AND THE SM. FOR EACH SLOPE PARAMETER, THE ESTIMATED STANDARD DEVIATIONS σ , t -STATISTICS, AND p -VALUES ARE SHOWN. THE COEFFICIENTS OF DETERMINATION R^2 ARE ALSO SHOWN

(a) TBM with fixed exponents: $\widehat{\text{AGB}}_{\text{Re}} = K' \cdot \Delta h^{1.25} \cdot \eta_0^{2.64}$,
 $\widehat{\text{AGB}}_{\text{Kr}} = K' \cdot \Delta h^{1.25} \cdot \eta_0^{1.16}$

Nr	Site	K'	σ	t	p	R^2	Nr	Site	D	σ	t	p	R^2
1	Remningstorp	7.6	0.20	37.2	2.7e-27	0.78	1	Remningstorp	9.0	0.40	22.2	1.4e-20	0.40
2		7.5	0.21	35.5	3.4e-24	0.80	2		9.1	0.45	20.2	7.8e-18	0.41
3		8.0	0.23	34.2	9.1e-24	0.79	3		9.4	0.44	21.2	2.3e-18	0.46
4		10.2	0.55	18.5	3.0e-17	0.22	4		8.3	0.53	15.6	2.4e-15	-0.07
5		8.8	0.32	27.8	5.9e-22	0.64	5		8.4	0.49	17.4	1.5e-16	0.13
6		7.1	0.23	30.3	3.4e-18	0.81	6		9.4	0.48	19.3	2.1e-14	0.54
7		7.1	0.18	39.3	2.1e-20	0.88	7		9.6	0.45	21.6	2.5e-15	0.63
8		7.2	0.25	28.5	1.1e-17	0.78	8		9.6	0.50	19.4	1.9e-14	0.54
9	Krycklan	6.7	0.19	36.3	4.4e-25	0.84	9	Krycklan	11.5	0.31	36.6	3.6e-25	0.85
10		6.6	0.18	36.1	5.1e-25	0.84	10		11.4	0.32	36.0	5.3e-25	0.84
11		6.8	0.18	37.4	1.9e-25	0.85	11		11.7	0.31	37.6	1.6e-25	0.85
12		6.7	0.17	39.5	4.1e-26	0.87	12		11.6	0.29	39.4	4.7e-26	0.87
13		7.5	0.22	34.0	2.6e-24	0.81	13		11.3	0.32	35.4	8.7e-25	0.82
14		7.4	0.22	34.4	1.8e-24	0.81	14		11.4	0.32	35.1	1.1e-24	0.82
15		7.3	0.21	35.2	9.8e-25	0.82	15		11.4	0.32	35.5	8.2e-25	0.83
16		7.0	0.20	34.9	1.2e-24	0.81	16		11.8	0.34	35.2	9.8e-25	0.81
17		7.2	0.19	37.7	1.5e-25	0.83	17		12.2	0.32	38.3	9.8e-26	0.84
18	6.8	0.19	35.9	5.7e-25	0.82	18	11.9	0.32	36.6	3.3e-25	0.83		

Color coding for acquisition number by HOA: 30 m 40 m 50 m 60 m

show that fixed exponents provide a more stable model. The choice of exact parameter values is not of primary interest to this paper.

D. Plot/Stand-Level Biomass Estimation

In Fig. 6, scatter plots showing the results of biomass estimation with the TBM and the SM are presented. Model parameters estimated using the same data are used. Error bars are also included, to show the uncertainty of the estimates. It can be observed that only for the Remningstorp acquisitions from 2012

fixing of the exponents in the TBM significantly decreases model performance, which can be also observed by comparing the R^2 -values in Table II and Table III(a). The SM performs poorer in Remningstorp than in Krycklan.

Both residual and prediction RMSE values are shown in Table IV for the TBM, in Table V for the TBM with fixed exponents, and in Table VI for the SM. As expected, the performance of the TBM is poorer in across-site evaluation and for large difference in HOA in Remningstorp, primarily due to the differences in the exponent β . It can also be observed that the TBM with fixed exponents gives a much lower and more

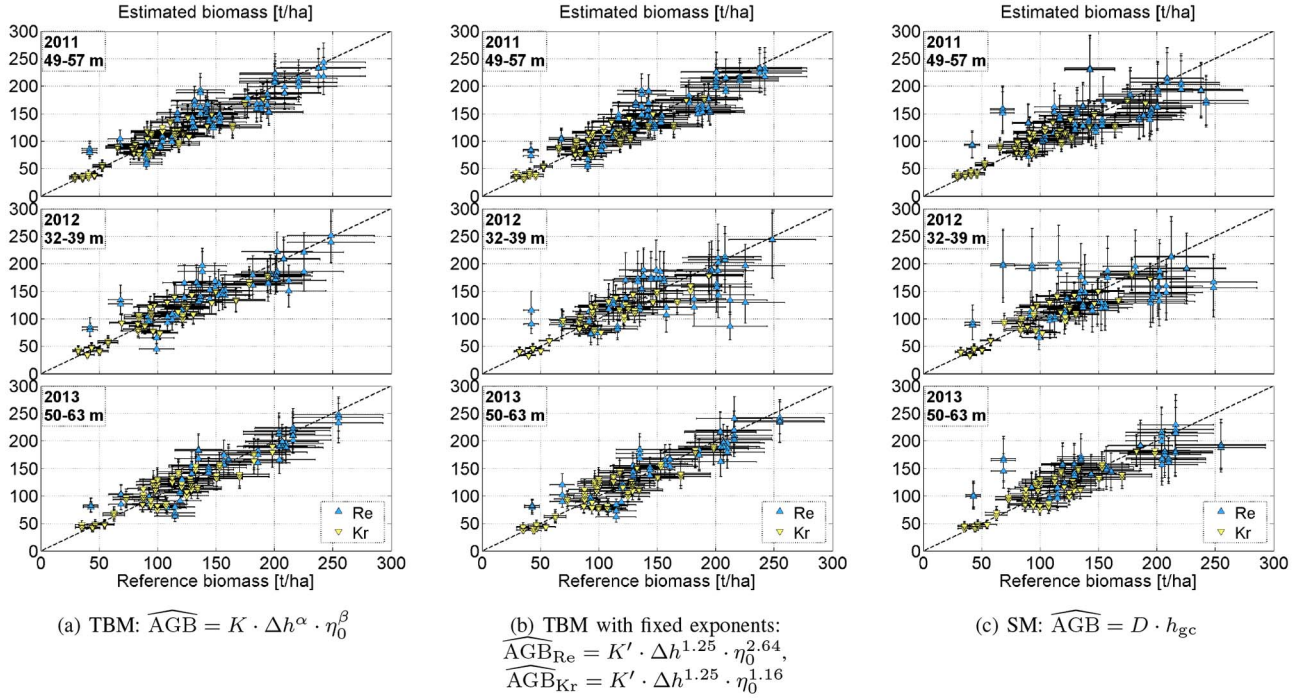


Fig. 6. Scatter plots showing biomass estimation results for models with parameters estimated from the same data. Acquisition year and HOA intervals are shown for each subplot. Error bars show $\pm 1\sigma$ confidence intervals of the estimates; for the horizontal bars, $\sigma = 15\%$, whereas for the vertical bars, σ equals the RMSE values shown on the diagonal of Tables IV–VI. The points shown represent 0.5-ha plots in Remningstorp and 2.4–26.3-ha stands in Krycklan. Note that several points may overlap. In Remningstorp, there are 88 points in 2011, 58 points in 2012, and 63 points in 2013, whereas in Krycklan, there are 116 points in 2011 and 87 points in both 2012 and 2013.

TABLE IV
RESIDUAL AND PREDICTION RMSE VALUES (IN PERCENT OF THE AVERAGE BIOMASS, WHICH CAN BE FOUND IN TABLE I) FOR THE TBM. RESIDUAL RMSE VALUES ARE MARKED IN BOLDFACE CHARACTERS AND SHOWN ON THE DIAGONAL. PREDICTION RMSE VALUES ARE SHOWN OFF-DIAGONAL.

TBM: $\widehat{AGB} = K \cdot \Delta h^\alpha \cdot \eta_0^\beta$ (K , α , and β as in Table II)

Training data		Validation data																	
Nr	Site	Remningstorp								Krycklan									
1	Remningstorp	16	15	16	39	25	17	14	17	46	43	45	41	48	47	46	43	50	44
2		16	15	16	41	26	17	14	16	48	45	48	43	50	49	48	45	52	46
3		18	17	15	38	25	23	21	20	41	37	40	35	41	40	39	37	45	39
4		68	72	68	19	33	73	77	80	29	29	31	30	39	38	37	33	33	30
5		29	31	29	27	16	32	33	36	35	33	36	33	43	42	41	36	39	34
6		17	16	19	41	27	15	12	17	48	45	48	44	51	50	49	46	52	46
7		17	17	20	44	30	16	12	16	53	50	53	49	55	55	54	51	56	51
8		17	16	19	44	30	17	14	15	51	47	50	45	51	51	49	47	55	48
9	Krycklan	32	33	29	24	23	33	34	35	15	16	15	15	19	18	17	16	16	16
10		31	32	29	23	21	31	32	33	15	16	15	14	20	19	18	17	17	16
11		32	33	30	24	23	34	34	35	15	16	15	15	19	18	17	16	16	16
12		32	33	31	23	22	32	33	35	15	16	15	14	19	19	18	16	16	15
13		53	55	52	26	35	52	55	56	23	23	21	20	16	16	16	18	18	21
14		50	51	49	25	33	49	51	52	22	22	20	19	16	16	16	17	17	20
15		46	47	45	24	30	47	49	50	19	20	18	18	16	16	16	17	15	18
16		35	36	34	23	24	35	36	37	16	17	16	15	18	17	17	16	15	16
17		36	37	33	26	27	38	38	39	17	19	16	18	18	18	17	17	14	17
18		31	32	30	23	22	31	32	33	16	16	15	14	19	18	18	16	16	15

Main color coding by RMSE value:

20%	40%	60%	80%
-----	-----	-----	-----

 Color coding for the acquisition number by HOA:

30 m	40 m	50 m	60 m
------	------	------	------

stable prediction RMSE without increasing the residual RMSE significantly. In the case of the SM, both residual and prediction RMSEs are low in Krycklan but higher in Remningstorp and across sites.

In Fig. 7, the dependence of the RMSE for the TBM on the parameters K , α , and β is studied. The default values of the parameters are $K = 7.42$, $\alpha = 1.25$, and $\beta = 2.64$ for Remningstorp and $\beta = 1.16$ for Krycklan, and they are marked

TABLE V
RESIDUAL AND PREDICTION RMSE VALUES (IN PERCENT OF THE AVERAGE BIOMASS, WHICH CAN BE FOUND IN TABLE I) FOR THE TBM WITH FIXED EXPONENTS. RESIDUAL RMSE VALUES ARE MARKED IN BOLDFACE CHARACTERS AND SHOWN ON THE DIAGONAL. PREDICTION RMSE VALUES ARE SHOWN OFF-DIAGONAL.

TBM with fixed exponents: $\widehat{AGB}_{Re} = K' \cdot \Delta h^{1.25} \cdot \eta_0^{2.64}$, $\widehat{AGB}_{Kr} = K' \cdot \Delta h^{1.25} \cdot \eta_0^{1.16}$ (K' as in Table III(a))

Training data		Validation data																	
Nr	Site	1	2	3	4	5	6	7	8	9	10	11	12	13	14	15	16	17	18
		Remningstorp								Krycklan									
1	Remningstorp	16	15	17	39	24	17	14	17	21	22	19	20	17	16	16	18	16	20
2		16	15	17	39	25	17	14	17	20	21	19	19	16	16	16	18	16	19
3		17	16	16	36	22	20	18	20	25	27	24	24	18	18	18	21	19	24
4		40	40	33	29	26	48	48	47	57	60	56	57	42	43	44	51	47	56
5		23	23	19	32	20	29	28	29	36	38	35	36	25	26	26	31	28	35
6		17	16	19	42	28	15	12	16	17	17	16	16	17	17	16	16	15	16
7		17	17	20	42	28	15	12	17	17	17	16	15	17	17	16	16	15	16
8		16	16	19	42	27	15	12	16	17	18	16	16	17	16	16	16	15	17
9	Krycklan	19	19	23	45	31	17	13	18	15	16	15	14	19	19	18	17	16	16
10		20	20	24	46	32	17	14	18	16	16	15	14	20	20	19	17	17	16
11		19	18	22	45	31	16	13	17	16	16	15	14	19	18	18	16	16	16
12		19	19	23	45	31	17	13	18	15	16	15	14	19	19	18	17	16	16
13		16	15	17	40	25	16	13	17	19	20	18	18	16	16	16	17	15	19
14		16	15	18	40	26	16	13	17	19	20	18	18	16	16	16	17	15	18
15		16	16	18	41	26	16	13	17	18	19	17	17	17	16	16	17	15	18
16		17	17	20	43	29	16	12	17	16	17	15	15	18	17	17	16	15	16
17		16	16	19	42	27	15	12	16	17	18	16	16	17	17	16	16	15	17
18		19	19	22	45	31	16	13	18	16	16	15	14	19	19	18	16	16	16

Main color coding by RMSE value:

20%	40%	60%	80%
-----	-----	-----	-----

Color coding for the acquisition number by HOA:

30 m	40 m	50 m	60 m
------	------	------	------

TABLE VI
RESIDUAL AND PREDICTION RMSE VALUES (IN PERCENT OF THE AVERAGE BIOMASS, WHICH CAN BE FOUND IN TABLE I) FOR THE SM. RESIDUAL RMSE VALUES ARE MARKED IN BOLDFACE CHARACTERS AND SHOWN ON THE DIAGONAL. PREDICTION RMSE VALUES ARE SHOWN OFF-DIAGONAL.

SM: $\widehat{AGB} = D \cdot h_{gc}$ (D as in Table III(b))

Training data		Validation data																	
Nr	Site	1	2	3	4	5	6	7	8	9	10	11	12	13	14	15	16	17	18
		Remningstorp								Krycklan									
1	Remningstorp	26	26	26	35	31	24	23	25	28	27	29	28	27	28	28	30	32	30
2		26	26	25	35	32	24	22	24	26	26	28	27	26	26	27	29	30	29
3		26	27	25	36	33	24	22	24	24	24	25	25	24	24	24	27	28	27
4		27	28	28	34	31	27	26	28	33	33	34	34	32	33	33	35	37	35
5		26	27	27	34	31	26	25	27	32	31	33	32	31	32	32	34	36	34
6		26	26	25	36	32	24	22	24	25	24	26	25	24	25	25	27	29	27
7		27	27	25	37	34	24	21	24	23	23	24	23	22	23	23	25	27	25
8		27	27	25	37	34	24	21	24	23	22	24	23	22	23	23	25	27	25
9	Krycklan	38	37	34	51	47	33	29	31	15	16	15	14	16	16	16	16	16	16
10		37	36	33	50	46	33	29	30	15	16	15	14	16	16	16	16	16	16
11		40	39	35	53	49	35	31	32	16	16	15	14	16	16	16	16	15	15
12		39	38	35	52	48	34	30	32	15	16	15	14	16	16	16	16	15	15
13		37	36	32	49	46	32	28	30	15	16	15	15	16	16	16	17	17	16
14		38	37	33	50	47	33	29	30	15	16	15	14	16	16	16	16	16	16
15		38	37	33	51	47	33	29	31	15	16	15	14	16	16	16	16	16	16
16		42	40	36	54	51	36	32	34	16	16	15	14	17	16	16	16	15	15
17		45	43	39	58	54	40	35	36	17	18	16	15	18	18	17	16	15	15
18		42	41	37	55	51	37	33	34	16	16	15	15	17	17	16	16	15	15

Main color coding by RMSE value:

20%	40%	60%	80%
-----	-----	-----	-----

Color coding for the acquisition number by HOA:

30 m	40 m	50 m	60 m
------	------	------	------

with vertical lines. [The default values for α and β have been chosen as described in Section IV-C, whereas the default value for K has been chosen to be the average of all K values in Table III(a).] Each parameter is varied around its default value, and the RMSE is computed. When one parameter is varied, the other two are held constant at their default values. Remningstorp and Krycklan are shown separately, and color

coding according to HOA has been applied. Note the significant difference between Remningstorp and Krycklan in model sensitivity to different parameter settings at different HOAs.

E. Biomass Mapping

In Fig. 8, biomass maps obtained using the TBM and SM are shown for both Remningstorp and Krycklan and compared

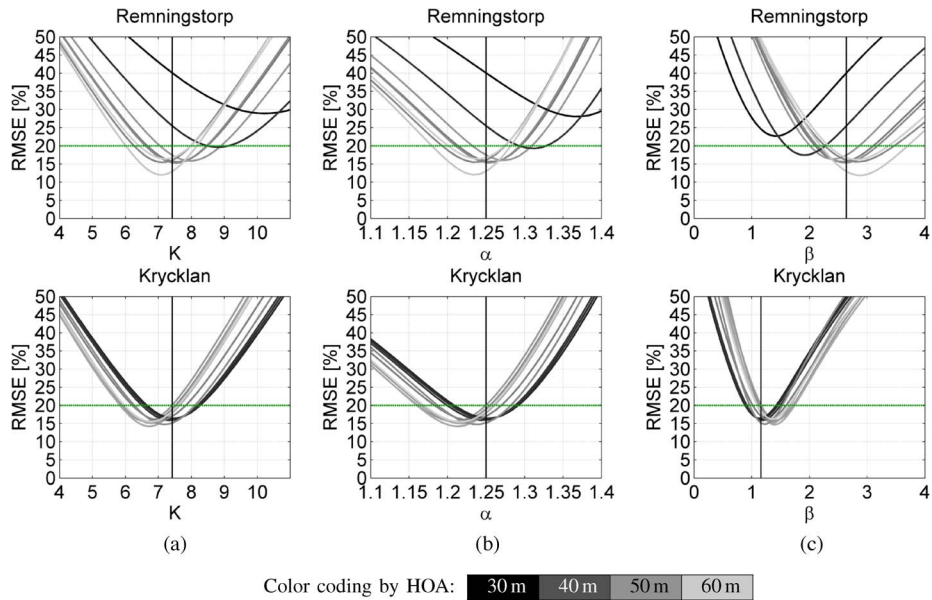


Fig. 7. Sensitivity of the TBM to small changes of parameters K , α , and β around a default setup with $\alpha = 1.25$, $\beta = 2.64$ for Remningstorp, $\beta = 1.16$ for Krycklan, and $K = 7.42$ [being the mean of all K' -values in Table III(a)]. The vertical lines show the default values, and the horizontal lines mark a 20–error level. (a) Sensitivity to K . (b) Sensitivity to α . (c) Sensitivity to β .

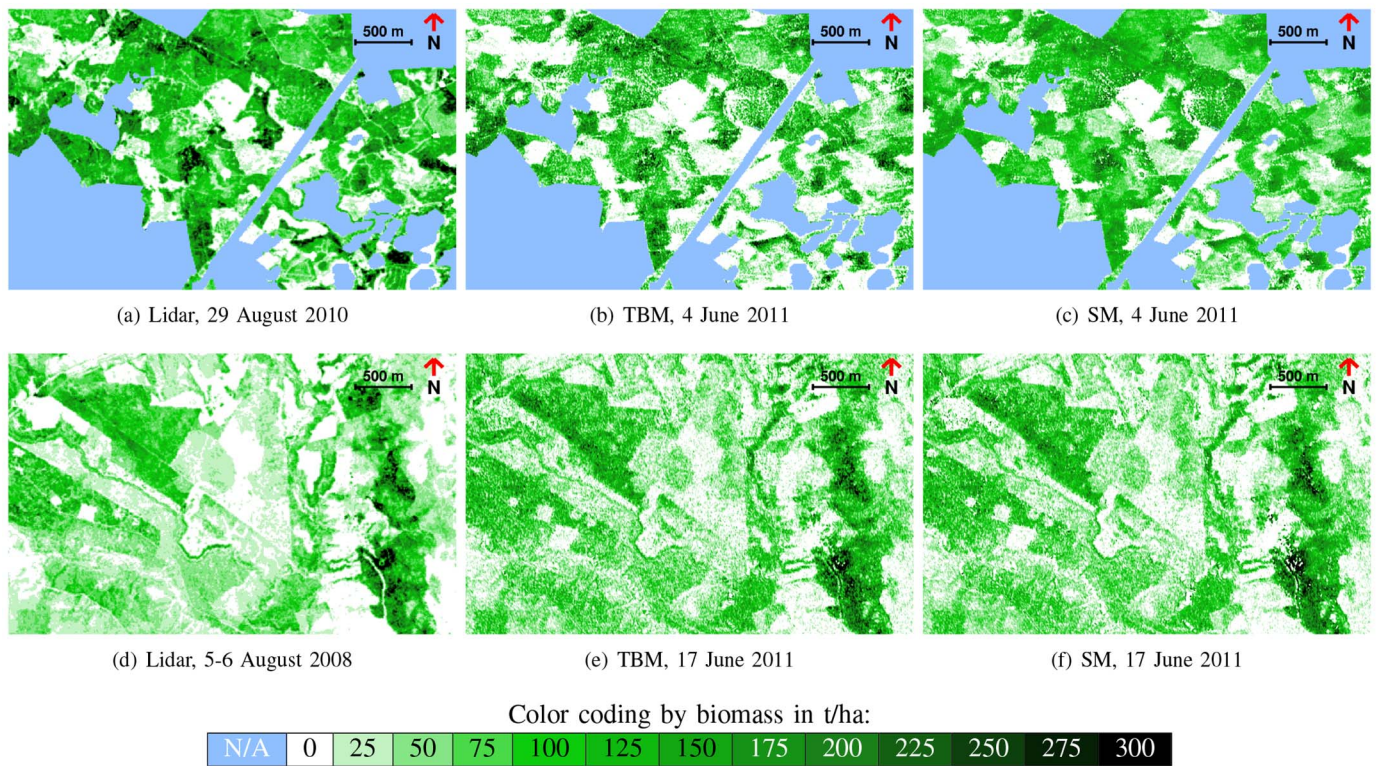


Fig. 8. Mapping results for (a)–(c) Remningstorp and (d)–(f) Krycklan. The lidar biomass maps are compared with biomass maps obtained using the TBM and the SM with single TDM image pairs from the corresponding dates. Model parameters estimated using the corresponding plot/stand-level estimates data are used. Note that growth has not been modeled in the lidar maps.

with lidar-derived biomass maps. For both test sites, the first acquisition from 2011 has been used: nr 1 for Remningstorp and nr 9 for Krycklan, together with the respective parameters presented in Tables II and III(b). Note that forest management procedures may have been conducted between the acquisition

of the lidar and the TDM data. Note also that, in Remningstorp, regions not covered by lidar scanning have been masked out.

As observed earlier, the TBM performs well both in Remningstorp and in Krycklan if the parameters obtained from acquisitions made at similar HOA and within the same test

site are used. Although the SM performs well in Krycklan, it can be observed that it cannot reproduce the biomass variance observed in Remningstorp.

V. DISCUSSION

The TBM is able to explain 65%–89% of the variance observed in data, with a residual RMSE of 12%–19% of the mean biomass, for 18 TDM images acquired over two test sites in Sweden. In cases when different data are used for training and validation, the model shows poorer results, with a prediction RMSE often exceeding 30% in across-site scenarios or when the difference in HOA is large. However, the TBM can be stabilized by fixing α and by letting β be a site-dependent constant. In that case, the prediction RMSE is below 20% for most of the acquisitions.

The TBM is here compared with a linear zero-intercept model, which scales the interferometric height to biomass. This scaling model (SM) has earlier been used in [22], where a stand-level residual RMSE of 19% has been obtained for a Norwegian test site using two images: one from the ascending orbit and one from the descending orbit, with the respective HOAs of 23 and 122 m. In [22], the scaling factor has been estimated to 14 t/ha/m, whereas in this paper, the same factor is between 8.3 and 9.6 for Remningstorp and between 11.3 and 12.2 for Krycklan. A method for biomass change detection has also been proposed in [22], based on direct scaling of the change in the interferometric height to change in biomass, without the need for a high-resolution DTM. From the results of this paper, it can be concluded that whereas Krycklan shows many similarities with the Norwegian test site, Remningstorp appears to be significantly different. The dependence of the interferometric height on HOA and the horizontal forest structure is particularly large in Remningstorp, and the model presented in [22] does not function well in this test site.

In [24], an approach based on the IWCM and multitemporal averaging of stand-level biomass estimates from 18 acquisitions made over Remningstorp at HOAs between 49 and 358 m, in both summer and winter, gives an RMSE of 16%, whereas multitemporal averaging of seven images acquired at temperatures below 3 °C gives an RMSE of 14%. In the case of a single image, the RMSE is in the interval 17%–33%. Additionally, a penetration depth (PD) model is introduced in [24], which uses a height-to-biomass allometric equation to compute biomass from the sum of the interferometric height and the PD. The PD-based approach gives RMSE values in the interval 18%–33%. The PD is the only parameter that needs to be estimated (the allometric relation is assumed known). However, the model does not account for the horizontal structure of the forest, which can be problematic in the case of a commercial forest, where management activities such as thinnings and clearings affect the denseness of the forest and its biomass but not necessarily its height.

In [25], an approach based on multiple regression of the interferometric height and the ground-corrected coherence, and their transformed versions, results in an RMSE of 14% for one TDM image acquired over Krycklan (nr 9 in Table I) and 17% for one TDM image acquired over Remningstorp (nr 1 in

Table I). The approach presented in [25] is based on multiple regression of interferometric observables, and the results may not be representative, particularly considering the limited extent of the data used in the paper.

A. TLM Inversion Aspects and Forest Structure Influence

As biomass predictors, the TBM uses two parameters obtained from the inversion of a two-level model (TLM). The inversion of the TLM requires a high-resolution DTM, and it is based on the assumption that volume decorrelation is the dominant decorrelation effect. In Sweden, there is a lidar DTM covering the whole country, and similar products are or will soon be available in many other countries. Therefore, the presented approach can already be used in many regions and on a large scale, as the global TDM data used for DEM generation have been made available by the DLR for scientific use. Since ground surface is temporally stable in most forested areas, the availability of high-resolution DTMs will only increase with time. The exact requirements on the DTM have not been studied here, but it is possible that a coarser DTM can be sufficient, as exemplified in [22]. Other techniques, such as P- and L-band InSAR, may also provide ground reference. These questions are left for follow-up studies.

In the presented approach, volume decorrelation has been assumed the dominant decorrelation effect. In the case of the single-pass interferometric bistatic-mode TDM data used here, the most significant decorrelation sources other than volume effects are the thermal noise and system imperfections. These effects have been ignored throughout this paper to keep the inversion process simple.

However, it has been observed in [26] that the TLM inversion provides unrealistically high Δh for clear cuts, and that the inverted level distance Δh is affected by a HOA-dependent offset. In Fig. 5(a), a change of slope has been observed for low H95. Additionally, a HOA dependence has been observed in the estimated model parameters α , β , and K presented in Table II, and that this dependence is stronger in Remningstorp, where the forest is taller and the relative HOA is lower.

A probable cause for these effects is that the SNR and system decorrelation effects have not been considered in the TLM inversion process. Since the interferometric phase has been calibrated using nonforested areas, the complex correlation coefficient for low forest and open areas has a high yet nonunitary real part and low imaginary part. The TLM cannot model a complex correlation coefficient with high coherence and low phase without making Δh close to HOA/2. This introduces a HOA-dependent offset in the estimated Δh .

A solution for this issue can be obtained through the modeling of a real-valued system and SNR decorrelation term γ_s , and replacing $\tilde{\gamma}_{gc}$ by $\tilde{\gamma}_{gc}/\gamma_s$ in (16), (15), and (17). If γ_s can be estimated, e.g., from the data, then an improvement of the TLM inversion performance can be expected. A second probable cause for these effects is that, at low HOA relative forest height, the modeling of the exact vertical distribution of scatterers becomes more important as the phase change with height is larger. The assumption of two scattering levels may then become too simplistic. Nevertheless, the issues related

to HOA dependence can be avoided in practical use by a sensible choice of HOA. Moreover, η_0 can often compensate for the large Δh , as observed for Remningstorp in Fig. 8, where biomass mapping in open fields is accurate.

As pointed out by an anonymous reviewer, the chosen representation of forest (two discrete scattering levels, the top one with gaps) gives a simple model that can be inverted directly, providing useful estimates of forest properties. However, as pointed out in [69], the same forest can also be represented using an extended volume over thin ground and without gaps. The main scope of this paper is not to propose the most suitable forest representation but rather to present a representation that is convenient for forest parameter estimation.

Although the proposed approach shows good potential in the two boreal test sites used in this paper, the TLM inversion may provide misleading results in very dense forests or forests with multilayer structure, for which the inverted TLM parameters may not be good metrics of forest height and canopy density. It is therefore important to consider the structure of the forest prior to using the proposed approach. Further studies are needed to evaluate the potential of the proposed approach in forests with other canopy structures.

An interesting observation can be made about the estimated values for the exponent β , associated with the canopy density estimate η_0 , which changes significantly between Remningstorp and Krycklan. This can be explained by the different structure of the trees in Remningstorp and in Krycklan. Using the Heureka system, it can be estimated that 68% of the total biomass in the 32 plots in Remningstorp is confined to the stem, whereas the same number is 76% for the 31 stands in Krycklan. In [70], it is concluded that the trees in Northern Sweden generally have smaller crowns than in Southern Sweden. A larger β in Remningstorp will compensate for the fact that the forest in Remningstorp has in general denser canopies, at similar biomass and height. This does also explain the better performance of the SM in Krycklan, where the influence of the canopy density estimate η_0 is lower.

B. Future Development

There is an ongoing debate about the mechanisms of microwave penetration into forest canopy, and whether the significant penetration of X-band SAR into the canopy is primarily due to the dielectric penetration through the scatterers or penetration through the canopy gaps [71]. In this paper, it is shown that the inclusion of canopy gaps in an interferometric model can be beneficial for model inversion, but the dielectric penetration has been disregarded, and further discussion on the penetration mechanisms is left for future studies.

The TLM can be used to study temporal change of canopy density from multitemporal single-pass InSAR acquisitions. By keeping Δh constant for all acquisitions and letting μ vary, an overdetermined equation system is obtained. A time-series study of η_0 can provide information on the change of the canopy density, due to seasonal variations, management procedures (e.g., clearing, thinning, and clear-cutting), or natural disasters, and, eventually, biomass change can be estimated as well.

The presented approach has been evaluated on VV-polarized X-band SAR data. An evaluation of this approach on other frequencies, for instance at C-band or L-band, is of large interest, but it currently cannot be done due to the lack of suitable systems. Moreover, due to the lack of suitable data at the time of writing of this paper, an evaluation of the proposed approach on other polarizations has not been done, and it is left for future studies. However, the presented approach is principally not restricted to the used frequency or polarization, although the TLM inversion process may need to be revisited in the future, where a different choice of ρ may be motivated. Moreover, as shown in [21], the difference between the interferometric height at HH-polarization and VV-polarization can be several meters. Although the exact relation between the inverted parameters Δh and η_0 and the lidar estimates of forest height and canopy density, as well as biomass, will most likely be different at other polarizations and frequencies, the presented approach may still be useful.

This paper has been restricted to data acquired at a 41° nominal angle of incidence. The influence of the incidence angle requires a separate study. An evaluation of the presented approach on tropical forest is also of interest. As the tropical forest is, in general, taller and denser, the penetration through canopy gaps is expected to be lower, which certainly will affect TLM inversion.

VI. CONCLUSION

A new biomass model is proposed, in which biomass is estimated from forest height and canopy density estimates obtained from two-level model (TLM) inversion using single-pass interferometric SAR data. In this paper, bistatic-mode, VV-polarized TDM data acquired at a 41° nominal incidence angle and with HOAs within 32–63 m over two Swedish test sites separated by 720 km are used together with a national DTM with a grid posting of 2 m × 2 m and vertical accuracy better than 0.5 m. Compared with other studies, the presented approach has provided similar or better results in terms of biomass retrieval, a larger data set has been used for the evaluation, and across-site and across-acquisition biomass retrieval scenarios have been studied.

It is here concluded that the two test sites used in this paper feature quite different forest, and regional training of the new model is required in operational use. However, only one of the three model parameters has been found significantly dependent on the test site, and the regional model training can be done using only a few data points, e.g., from the NFI database. The HOA-dependent bias, most likely caused primarily by the lack of system and SNR decorrelation modeling, can be suppressed either by choosing HOAs larger than approximately twice the forest height (typically around 40–60 m), which is the case for most of the global TDM acquisitions over boreal forests, or by the modeling of a real-valued system and SNR decorrelation term.

Since a high-resolution DTM is required for TLM inversion and the model has only been evaluated on boreal forests, the presented approach is suitable for frequent mapping of large areas of boreal forest in regions with known topography. Since

the ground surface is most often temporally stable in forested regions, only one DTM acquisition is required. Thereafter, forest height, canopy density, and biomass mapping can be done using spaceborne SAR with large coverage, high resolution, and frequent acquisitions. Therefore, the presented approach is useful for the monitoring of national forest resources, and for improved forest management. With an access to the global TDM data, national maps of forest height, canopy density, and biomass can be created.

ACKNOWLEDGMENT

The authors would like to thank the German Aerospace Center (DLR) for the TDM data and support provided within proposal XTI_VEGE0376, the Swedish Land Survey for the DTM and SPOT-5 data, Skogssällskapet for the information on forest management activities, the European Space Agency (ESA) for the lidar data from the BioSAR 2008 and 2010 campaigns, and the anonymous reviewers and the faculty opponents and evaluation committees for M. J. Soja's and H. J. Persson's Ph.D. defences, for their valuable input to this paper.

REFERENCES

- [1] IPCC, *Climate Change 2007: The Physical Science Basis. Contribution of Working Group I to the Fourth Assessment Report of the Intergovernmental Panel on Climate Change*, S. Solomon, D. Qin, M. Manning, Z. Chen, M. Marquis, K. B. Averyt, M. Tignor, and H. L. Miller, Eds. Cambridge, U.K.: Cambridge Univ. Press, 2007.
- [2] S. H. Spurr, *Aerial Photographs in Forestry*. New York, NY, USA: Ronal Press Company, 1948.
- [3] J. Hyypä *et al.*, "Accuracy comparison of various remote sensing data sources in the retrieval of forest stand attributes," *Forest Ecol. Manage.*, vol. 128, no. 1/2, pp. 109–120, Mar. 2000.
- [4] B. St-Onge, Y. Hu, and C. Vega, "Mapping the height and above-ground biomass of a mixed forest using lidar and stereo Ikonos images," *Int. J. Remote Sens.*, vol. 29, no. 5, pp. 1277–1294, Mar. 2008.
- [5] H. Persson, J. Wallerman, H. Olsson, and J. E. Fransson, "Estimating forest biomass and height using optical stereo satellite data and a DTM from laser scanning data," *Can. J. Remote Sens.*, vol. 39, no. 3, pp. 251–262, Sep. 2013.
- [6] M. Nilsson, "Estimation of tree heights and stand volume using an airborne lidar system," *Remote Sens. Environ.*, vol. 56, no. 1, pp. 1–7, Apr. 1996.
- [7] J. Hyypä *et al.*, "Review of methods of small-footprint airborne laser scanning for extracting forest inventory data in boreal forests," *Int. J. Remote Sens.*, vol. 29, no. 5, pp. 1339–1366, Mar. 2008.
- [8] E. Næsset *et al.*, "Laser scanning of forest resources: The nordic experience," *Scand. J. Forest Res.*, vol. 19, no. 6, pp. 482–499, Dec. 2004.
- [9] S. C. Popescu, "Estimating biomass of individual pine trees using airborne lidar," *Biomass Bioenergy*, vol. 31, no. 9, pp. 646–655, Sep. 2007.
- [10] E. Næsset *et al.*, "Model-assisted regional forest biomass estimation using lidar and InSAR as auxiliary data: A case study from a boreal forest area," *Remote Sens. Environ.*, vol. 115, no. 12, pp. 3599–3614, Dec. 2011.
- [11] M. A. Lefsky *et al.*, "Estimates of forest canopy height and aboveground biomass using ICESat," *Geophys. Res. Lett.*, vol. 32, no. 22, Nov. 2005, Art. ID. L22S02.
- [12] K. J. Ranson *et al.*, "Mapping of boreal forest biomass from spaceborne synthetic aperture radar," *J. Geophys. Res.*, vol. 102, no. D24, pp. 29 599–29 610, Dec. 1997.
- [13] B. Koch, "Status and future of laser scanning, synthetic aperture radar and hyperspectral remote sensing data for forest biomass assessment," *ISPRS J. Photogramm. Remote Sens.*, vol. 65, no. 6, pp. 581–590, Nov. 2010.
- [14] R. Bamler and P. Hartl, "Synthetic aperture radar interferometry," *Inverse Probl.*, vol. 14, no. 4, pp. R1–R54, 1998.
- [15] Produktbeskrivning: GSD-Höjddata, grid 2+, (in Swedish), Swedish Land Survey (Lantmäteriet), Gävle, Sweden, Tech. Rep., 2013.
- [16] J. Kellndorfer *et al.*, "Vegetation height estimation from shuttle radar topography mission and national elevation datasets," *Remote Sens. Environ.*, vol. 93, no. 3, pp. 339–358, Nov. 2004.
- [17] L. W. Kenyi, R. Dubayah, M. Hofton, and M. Schardt, "Comparative analysis of SRTM-NED vegetation canopy height to LIDAR-derived vegetation canopy metrics," *Int. J. Remote Sens.*, vol. 30, no. 11, pp. 2797–2811, Jun. 2009.
- [18] S. Solberg, R. Astrup, O. M. Bollandsås, E. Næsset, and D. J. Weydahl, "Deriving forest monitoring variables from X-band InSAR SRTM height," *Can. J. Remote Sens.*, vol. 36, no. 1, pp. 68–79, Jan. 2010.
- [19] T. G. Farr *et al.*, "The shuttle radar topography mission," *Rev. Geophys.*, vol. 45, no. 2, Jun. 2007, Art. ID. RG2004.
- [20] J. Praks, O. Antropov, and M. T. Hallikainen, "LIDAR-aided SAR interferometry studies in boreal forest: Scattering phase center and extinction coefficient at X- and L-band," *IEEE Trans. Geosci. Remote Sens.*, vol. 50, no. 10, pp. 3831–3843, Oct. 2012.
- [21] F. Kugler, D. Schulze, I. Hajnsek, H. Pretzsch, and K. P. Papathanassiou, "TanDEM-X Pol-InSAR performance for forest height estimation," *IEEE Trans. Geosci. Remote Sens.*, vol. 52, no. 10, pp. 6404–6422, Oct. 2014.
- [22] S. Solberg, R. Astrup, J. Breidenbach, B. Nilsen, and D. Weydahl, "Monitoring spruce volume and biomass with InSAR data from TanDEM-X," *Remote Sens. Environ.*, vol. 139, pp. 60–67, Dec. 2013.
- [23] S. Solberg, R. Astrup, T. Gobakken, E. Næsset, and D. J. Weydahl, "Estimating spruce and pine biomass with interferometric X-band SAR," *Remote Sens. Environ.*, vol. 114, no. 10, pp. 2353–2360, Oct. 2010.
- [24] J. I. H. Askne, J. E. S. Fransson, M. Santoro, M. J. Soja, and L. M. H. Ulander, "Model-based biomass estimation of a hemi-boreal forest from multitemporal TanDEM-X acquisitions," *Remote Sens.*, vol. 5, no. 11, pp. 5574–5597, Oct. 2013.
- [25] H. Persson and J. E. S. Fransson, "Comparison between TanDEM-X and ALS based estimation of biomass and tree height in boreal forests," *Remote Sens. Environ.*, submitted for publication.
- [26] M. J. Soja and L. M. H. Ulander, "Two-level forest model inversion of interferometric TDM data," in *Proc. 10th EUSAR Conf.*, 2014, pp. 1137–1140.
- [27] M. J. Soja, H. Persson, and L. M. H. Ulander, "Estimation of forest height and canopy density from a single InSAR correlation coefficient," *IEEE Geosci. Remote Sens. Lett.*, vol. 12, no. 3, pp. 646–650, Mar. 2015.
- [28] H. Petersson, "Biomassfunktioner för trädfractioner av tall, gran och björk i Sverige," (in Swedish), SLU, Inst. Skoglig Resurshållning Geomatik, Arbetsrapport 59, Umeå, Sweden, Tech. Rep., 1999.
- [29] M. Cannell, "Woody biomass of forest stands," *Forest Ecol. Manage.*, vol. 8, no. 3/4, pp. 299–312, Jun. 1984.
- [30] J. Chave *et al.*, "Tree allometry and improved estimation of carbon stocks and balance in tropical forest," *Oecologia*, vol. 145, no. 1, pp. 87–99, Aug. 2005.
- [31] S. Brown, A. J. R. Gillespie, and A. E. Lugo, "Biomass estimation methods for tropical forests with applications to forest inventory data," *Forest Sci.*, vol. 35, no. 4, pp. 881–902, Dec. 1989.
- [32] D. Zianis, P. Muukkonen, R. Mäkipää, and M. Mencuccini, "Biomass and stem volume equations for tree species in Europe," in *Silva Fennica*, The Finnish Society of Forest Science, Amsterdam, The Netherlands: IOS Press, 2005.
- [33] E. Næsset, "Determination of mean tree height of forest stands using airborne laser scanner data," *ISPRS J. Photogramm. Remote Sens.*, vol. 52, no. 2, pp. 49–56, Apr. 1997.
- [34] J. Holmgren, "Estimation of forest variables using airborne laser scanning," Ph.D. dissertation, Dept. Forest Econ., Swedish Univ. Agric. Sci., Uppsala, Sweden, 2003, vol. 278, no. 2.
- [35] S. R. Cloude and K. P. Papathanassiou, "Polarimetric SAR interferometry," *IEEE Trans. Geosci. Remote Sens.*, vol. 36, no. 5, pp. 1551–1565, Sep. 1998.
- [36] K. P. Papathanassiou and S. R. Cloude, "Single-baseline polarimetric SAR interferometry," *IEEE Trans. Geosci. Remote Sens.*, vol. 39, no. 11, pp. 2352–2363, Nov. 2001.
- [37] S. R. Cloude and K. P. Papathanassiou, "Three-stage inversion process for polarimetric SAR interferometry," *Proc. Inst. Elect. Eng.—Radar, Sonar Navig.*, vol. 150, no. 3, pp. 125–134, Jun. 2003.
- [38] H. Raggam, K. Gutjahr, R. Perko, and M. Schardt, "Assessment of the stereo-radargrammetric mapping potential of TerraSAR-X multibeam spotlight data," *IEEE Trans. Geosci. Remote Sens.*, vol. 48, no. 2, pp. 971–977, Feb. 2010.
- [39] H. Persson and J. Fransson, "Forest variable estimation using radargrammetric processing of TerraSAR-X images in boreal forests," *Remote Sens.*, vol. 6, no. 3, pp. 2084–2107, Mar. 2014.
- [40] Y. Wu and A. H. Strahler, "Remote estimation of crown size, stand density, and biomass on the Oregon transect," *Ecol. Appl.*, vol. 4, no. 2, pp. 299–312, May 1994.

- [41] J. Zhou *et al.*, "Tree crown detection in high resolution optical and lidar images of tropical forest," in *Proc. SPIE*, 2010, vol. 7824, p. 78240Q.
- [42] S. A. Soenen, D. R. Peddle, R. J. Hall, C. A. Coburn, and F. G. Hall, "Estimating aboveground forest biomass from canopy reflectance model inversion in mountainous terrain," *Remote Sens. Environ.*, vol. 114, no. 7, pp. 1325–1337, Jul. 2010.
- [43] S. C. Popescu, R. H. Wynne, and R. F. Nelson, "Measuring individual tree crown diameter with lidar and assessing its influence on estimating forest volume and biomass," *Can. J. Remote Sens.*, vol. 29, no. 5, pp. 564–577, Oct. 2003.
- [44] S. C. Popescu and R. H. Wynne, "Seeing the trees in the forest: Using lidar and multispectral data fusion with local filtering and variable window size for estimating tree height," *Photogramm. Eng. Remote Sens.*, vol. 50, no. 5, pp. 589–604, May 2004.
- [45] Y. Ilvessalo, "On the correlation between the crown diameter and the stem of trees," *Metsätieteellisen tutkimuslaitoksen julkaisuja*, vol. 38, no. 2, pp. 1–32, 1950.
- [46] G. E. Hemery, P. S. Savill, and S. N. Pryor, "Applications of the crown diameter-stem diameter relationship for different species of broadleaved trees," *Forest Ecol. Manage.*, vol. 215, no. 1–3, pp. 285–294, Aug. 2005.
- [47] J. Kalliovirta and T. Tokola, "Functions for estimating stem diameter and tree age using tree height, crown width and existing stand database information," *Silva Fennica*, vol. 39, no. 2, pp. 227–248, 2005.
- [48] J.-S. Lee, K. W. Hoppel, S. A. Mango, and A. R. Miller, "Intensity and phase statistics of multilook polarimetric and interferometric SAR imagery," *IEEE Trans. Geosci. Remote Sens.*, vol. 32, no. 5, pp. 1017–1028, Sep. 1994.
- [49] E. Rodriguez and J. Martin, "Theory and design of interferometric synthetic aperture radars," *Proc. Inst. Elect. Eng. F—Radar Signal Process.*, vol. 139, no. 2, pp. 147–159, Apr. 1992.
- [50] H. Zebker and J. Villasenor, "Decorrelation in interferometric radar echoes," *IEEE Trans. Geosci. Remote Sens.*, vol. 30, no. 5, pp. 950–959, Sep. 1992.
- [51] J. O. Hagberg, L. M. H. Ulander, and J. I. H. Askne, "Repeat-pass SAR interferometry over forested terrain," *IEEE Trans. Geosci. Remote Sens.*, vol. 33, no. 2, pp. 331–340, Mar. 1995.
- [52] J. Askne, P. Dammert, L. M. H. Ulander, and G. Smith, "C-band repeat-pass interferometric SAR observations of the forest," *IEEE Trans. Geosci. Remote Sens.*, vol. 35, no. 1, pp. 25–35, Jan. 1997.
- [53] M. J. Soja, H. Persson, and L. M. H. Ulander, "Estimation of boreal forest biomass from two-level model inversion of interferometric TanDEM-X data," in *Proc. IEEE IGARSS*, Quebec, QC, Canada, 2014, pp. 3398–3401.
- [54] J. Askne, M. Santoro, G. Smith, and J. E. S. Fransson, "Multitemporal repeat-pass SAR interferometry of boreal forests," *IEEE Trans. Geosci. Remote Sens.*, vol. 41, no. 7, pp. 1540–1550, Jun. 2003.
- [55] L. M. H. Ulander *et al.*, "BioSAR 2010: Technical assistance for the development of airborne SAR and geophysical measurements during the BioSAR 2010 experiment: Final report," ESA contract no. 4000102285/10/NL/JA/ef, European Space Agency (ESA), Paris, France, Tech. Rep., 2011.
- [56] G. Krieger *et al.*, "TanDEM-X: A satellite formation for high-resolution SAR interferometry," *IEEE Trans. Geosci. Remote Sens.*, vol. 45, no. 11, pp. 3317–3341, Nov. 2007.
- [57] S. Duque, U. Balss, C. Rossi, T. Fritz, and W. Balzer, "TanDEM-X payload ground segment, CoSSC generation and interferometric considerations," Remote Sens. Technol. Inst., German Aerosp. Center (DLR), Oberpfaffenhofen, Germany, Tech. Rep., 2012.
- [58] R Core Team, R: A Language and Environment for Statistical Computing. Vienna, Austria: R Foundation for Statistical Computing, 2013.
- [59] I. Hajnsek *et al.*, "BioSAR 2008 technical assistance for the development of airborne SAR and geophysical measurements during the BioSAR 2008 experiment: Final report—BioSAR campaign," ESA contract no. 22052/08/NL/CT, European Space Agency (ESA), Paris, France, Tech. Rep., 2009.
- [60] P. Wikström *et al.*, "The Heureka forestry decision support system: An overview," *Math. Comput. Forestry Nat.—Resource Sci.*, vol. 3, no. 2, pp. 87–94, 2011.
- [61] L. G. Marklund, "Biomassfunktioner för gran i Sverige," Inst. Skogstaxering, Sveriges Lantbruksuniversitet, Umeå, Sweden, Rapport 43, 1987.
- [62] L. G. Marklund, "Biomassfunktioner för tall, gran och björk i Sverige," Inst. Skogstaxering, Sveriges Lantbruksuniversitet, Umeå, Sweden, Rapport 45, 1988.
- [63] N. Fahlvik, B. Elfving, and P. Wikström, "Evaluation of growth models used in the Swedish forest planning system Heureka," *Silva Fennica*, vol. 48, no. 2, pp. 1–17, 2014.
- [64] G. Sandberg, L. M. H. Ulander, J. E. S. Fransson, J. Holmgren, and T. Le Toan, "L- and P-band backscatter intensity for biomass retrieval in hemiboreal forest," *Remote Sens. Environ.*, vol. 115, no. 11, pp. 2874–2886, Nov. 2011.
- [65] M. J. Soja, "Modelling and retrieval of forest parameters from synthetic aperture radar data," Chalmers Univ. Technol., Göteborg, Sweden, Tech. Rep., 2012.
- [66] P. Axelsson, "Processing of laser scanner data—Algorithms and applications," *ISPRS J. Photogramm. Remote Sens.*, vol. 54, no. 2/3, pp. 138–147, Jul. 1999.
- [67] P. Axelsson, "DEM generation from laser scanner data using adaptive TIN models," in *Proc. Int. Arch. Photogramm. Remote Sens.*, 2000, vol. 33, pp. 110–117.
- [68] M. J. Soja and L. M. H. Ulander, "Digital canopy model estimation from TDM interferometry using high-resolution lidar DEM," in *Proc. IEEE IGARSS*, Melbourne, Vic., Australia, 2013, pp. 165–168.
- [69] S. Tebaldini and F. Rocca, "Multibaseline polarimetric SAR tomography of a boreal forest at P- and L-bands," *IEEE Trans. Geosci. Remote Sens.*, vol. 50, no. 1, pp. 232–246, Jan. 2012.
- [70] A. Jakobsons, "The relationship between crown diameter and other tree factors, diameter at breast height in particular: Analysis based on the sample tree material of the national forest inventory," Stockholms Skoghögskolan, Insitutionen Skogstaxering, Stockholm, Sweden, Tech. Rep., 1970.
- [71] F. De Zan, G. Krieger, and P. Lopez-Dekker, "On some spectral properties of TanDEM-X interferograms over forested areas," *IEEE Geosci. Remote Sens. Lett.*, vol. 10, no. 1, pp. 71–75, Jan. 2013.



Maciej Jerzy Soja was born in Warsaw, Poland, in 1985. He received the M.Sc. degree in engineering physics and the Ph.D. degree in radio and space science from the Chalmers University of Technology, Gothenburg, Sweden, in 2009 and 2014, respectively.

He is currently a Postdoctoral Researcher with the Radar Remote Sensing Group, Department of Earth and Space Sciences, Chalmers University of Technology. He is active in several international projects, including the selected ESA P-band synthetic aperture radar (SAR) mission BIOMASS and the Advanced

SAR project, funded from European Commission's Seventh Framework Programme. His main research interests include SAR in forestry, electromagnetic modeling, and lidar scanning data analysis.



Henrik J. Persson received the M.Sc. degree in engineering physics from the Luleå University of Technology, Luleå, Sweden, in 2009 and the Ph.D. degree in forest remote sensing from the Swedish University of Agricultural Sciences, Umeå, Sweden, in 2014.

In between, he also had a two-year departure working at the Swiss Federal Institute of Technology (ETH), Zürich, Switzerland. He is currently working as a Researcher with the Forest Remote Sensing Section, Swedish University of Agricultural Sciences, where he is involved in both national and international projects, including the Advanced SAR and GlobBiomass projects. His main research interests include forest parameter modeling from satellite radar and optical data, and airborne laser scanning data.



Lars M. H. Ulander (S'86–M'90–SM'04) received the M.Sc. degree in engineering physics and the Ph.D. degree in electrical and computer engineering from the Chalmers University of Technology, Gothenburg, Sweden, in 1985 and 1991, respectively.

Since 1995, he has been with the Swedish Defence Research Agency (FOI), Linköping, Sweden, where he is currently the Director of Research in radar signal processing. He is currently a Professor of radar remote sensing with Chalmers University of Technology. He is the author or coauthor of over

300 professional publications, of which more than 60 are in peer-reviewed scientific journals. He is the holder of five patents. His research interests include synthetic aperture radar, electromagnetic scattering models, and remote sensing applications.

Corrections to “Estimation of Forest Biomass From Two-Level Model Inversion of Single-Pass InSAR Data”

Maciej Jerzy Soja, Henrik J. Persson, and Lars M. H. Ulander, *Senior Member, IEEE*

In the above paper [1], there are errors in Table I. The corrected table is published here.

TABLE I

SUMMARY FOR THE EXPERIMENTAL DATA USED IN THIS STUDY. MEAN VALUES FOR ALL PLOTS ARE GIVEN. BACKGROUND SHADING HAS BEEN APPLIED ACCORDING TO HOA. N IS THE NUMBER OF AVAILABLE PLOTS/STANDS FOR EACH ACQUISITION. NOTE THAT H95 HAS BEEN MEASURED IN 2010 AND GROWTH HAS NOT BEEN MODELED

Nr	Site	Date	InSAR data			<i>In situ</i> & lidar data						
			B_{\perp} [m]	HOA [m]	Coherence	N	Biomass [t/ha]			H95 [m]		
						min	mean	max	min	mean	max	
1	Remmingsstorp	20110604	282	49	0.65	32	42	148	242	14	23	32
2		20110809	266	52	0.67	28	42	150	242	14	23	32
3		20110820	258	54	0.66							
4		20120601	432	32	0.54	29	42	153	249	14	22	30
5		20120828	370	37	0.54							
6		20130702	270	51	0.66	21	43	158	255	14	22	30
7		20130724	226	61	0.73							
8		20130804	220	63	0.73							
9	Krycklan	20110617	258	52	0.71	29	29	102	191	7	16	21
10		20110720	250	54	0.75							
11		20110811	242	55	0.76							
12		20110822	240	56	0.78							
13		20120717	374	36	0.59							
14		20120808	360	37	0.61							
15		20120819	350	39	0.62							
16		20130601	270	50	0.73							
17		20130623	260	52	0.71							
18		20130726	216	62	0.79		35	110	198			

Color coding by HOA: 30 m 40 m 50 m 60 m

REFERENCES

- [1] M. J. Soja, H. J. Persson, and L. M. H. Ulander, “Estimation of forest biomass from two-level model inversion of single-pass InSAR data,” *IEEE Trans. Geosci. Remote Sens.*, vol. 53, no. 9, pp. 5083–5099, Sep. 2015.

Manuscript received June 18, 2015.

M. J. Soja is with the Department of Earth and Space Sciences, Chalmers University of Technology, 412 96 Gothenburg, Sweden (e-mail: maciej.soja@chalmers.se).

H. J. Persson is with the Department of Forest Resource Management, Swedish University of Agricultural Sciences, 901 83 Umeå, Sweden.

L. M. H. Ulander is with the Department of Earth and Space Sciences, Chalmers University of Technology, 412 96 Gothenburg, Sweden, and also with the Radar Systems Unit, Swedish Defence Research Agency (FOI), 581 11 Linköping, Sweden.

Digital Object Identifier 10.1109/TGRS.2015.2456836